Influence of macrophytes on stratification and dissolved oxygen dynamics in ponds

Ellen A. Albright[1,2], Robert Ladwig[2], and Grace M. Wilkinson[1,2]

[1] Iowa State University, Ames, Iowa, USA

[2] Center for Limnology, University of Wisconsin-Madison, Madison, Wisconsin, USA

ORCID numbers and contact information

Albright: 0000-0002-6226-9158 ealbright2@wisc.edu

Ladwig: 0000-0001-8443-1999 rladwig2@wisc.edu

Wilkinson: 0000-0003-4051-2249 gwilkinson@wisc.edu

Corresponding author: Ellen A. Albright (ealbright2@wisc.edu); 224 Hasler Laboratory of Limnology, 680 N. Park Street, Madison, WI 53706 USA

This manuscript has been submitted for publication in the Journal of Ecology. Please note that this manuscript has not yet undergone peer-review nor been formally accepted for publication. Subsequent versions of this manuscript may have slightly different content. If accepted, the final version of the manuscript will be available via the peer-reviewed publication DOI link at the top of this webpage. Please feel free to contact the corresponding author.

ABSTRACT

1. Small waterbodies are sensitive to stressors such as nutrient enrichment and heatwaves. However, when present, macrophytes may mediate these compounding stressors through their influence on water column thermal structure. Canopy-forming macrophyte beds can induce thermal stratification, which may limit the depth and degree of water column warming during heatwaves.
2. We leveraged an ecosystem experiment and hydrodynamic model to evaluate how macrophyte biomass, thermal structure, and dissolved oxygen (DO) responded to the interaction of episodic nutrient loading and periods of high temperatures in two shallow, temperate ponds (mean depth 0.8 m, maximum depth 2 m). We added nutrients to one pond, simulating storm-driven loading, while the other pond served as an unmanipulated reference. Following the first nutrient addition both ponds experienced a 5-day period of high surface water temperatures.
3. Submersed macrophytes in the nutrient addition pond began to senesce mid-summer, likely a result of phytoplankton shading from the nutrient addition and heat stress, while macrophytes in the reference pond followed expected seasonal patterns, senescing in early autumn.
4. We found that macrophytes structured the thermal environment in the ponds through vertical attenuation of turbulent kinetic energy and light. Macrophytes reduced the vertical extent of water column warming during the sustained heat event by 0.25-0.5 m and maintained cooler bottom temperatures (up to 2.5 °C cooler) throughout the summer, suggesting that macrophytes may buffer small waterbodies from heatwaves. Seasonal patterns in DO saturation also followed trends in macrophyte biomass; however, during the heat event, DO saturation fell sharply (declined by 22.4 to 50.4%) in both ponds and remained depressed through the remainder of the summer.

5. *Synthesis:* Our findings reveal that canopy-forming aquatic plant beds can buffer ponds from brief aquatic heat events but also that the plants themselves are sensitive to nutrient loading and temperature extremes. These results contribute to our mechanistic understanding of the effects of compound, extreme events in small waterbodies and the role aquatic plants can play in mediating these stressors. This understanding is necessary for adaptive management of small waterbodies such that these systems will continue to support freshwater biodiversity.

Keywords: dissolved oxygen, heatwaves, hydrodynamics, macrophytes, phenology, ponds, water temperature

INTRODUCTION

Small lakes and ponds are the most abundant lentic ecosystems worldwide and sites of critical importance for freshwater biodiversity and biogeochemical cycles (Scheffer et al., 2006; Cole et al., 2007; Messager et al., 2016). Small waterbodies are active components of regional- and global-scale carbon cycling, both as sites of burial and storage (Wilkinson et al., 2018; Taylor et al., 2019) and as sources of atmospheric carbon dioxide and methane (Holgerson & Raymond, 2016; Peacock et al., 2021). Small lakes and ponds enhance local and regional biodiversity, due in part to abundant macrophytes (Van Geest et al., 2003). Robust macrophyte communities support greater diversity of other taxa by providing food resources and habitat structure (Williams et al., 2004; Scheffer et al., 2006). In addition to these biotic interactions, macrophytes play a pivotal role in the ecosystem structure and function of small waterbodies. Interactions between hydrodynamics and the physical structure of macrophyte beds influence turbulent mixing, water column thermal structure, and sediment stability as well as whole-lake

productivity and nutrient cycling (Carpenter & Lodge, 1986; Scheffer et al., 1993; Licci et al., 2019). Despite the prevalence and importance of small, vegetated lakes and ponds, these ecosystems remain understudied (Downing, 2010; Biggs et al., 2017), particularly with regards to the role of macrophyte-hydrodynamic interactions in mediating ecosystem response to stressors.

The characteristic morphometry of small waterbodies makes these ecosystems more susceptible to stressors. For example, limited water volume and shallow mean depth reduce both dilution potential and thermal inertia making small waterbodies sensitive to nutrient loading and intense heatwaves (Biggs et al., 2017; Woolway et al., 2021a; Polazzo et al., 2022). As a result, eutrophication and aquatic heatwaves may act as compounding stressors for small lakes and ponds. Aquatic heatwaves are periods of sustained high surface water temperatures relative to local and seasonal baseline conditions (Hobday et al., 2016; Tassone et al., 2021; Woolway et al., 2021a). The frequency, duration, and intensity of aquatic heatwaves have increased over the past century with climate change, a trend which is anticipated to continue (Oliver et al., 2018; Woolway et al., 2021a, Woolway et al., 2022). Aquatic heatwaves may lower dissolved oxygen (DO) concentrations directly through reduced gas solubility in warmer waters and indirectly through increased ecosystem respiration (Tassone et al., 2021). Low DO concentrations and thermal stress have been linked to coral bleaching, declines in kelp forests, and mass seagrass mortality in marine systems (Wernberg et al., 2016; Hughes et al., 2017; Strydom et al., 2020). Although heatwaves are well-studied in coastal and marine systems, research on the effects of heatwaves in lakes and ponds is relatively nascent (Woolway et al., 2021a; Woolway et al., 2022). As such, it remains unclear how aquatic heatwaves affect the structure and function of lentic ecosystems, especially small, vegetated waterbodies.

Macrophytes may buffer small lakes and ponds from extreme temperatures by restricting vertical heat transfer. Canopy-forming macrophyte beds attenuate incoming solar radiation and dissipate wind-driven turbulence, thus limiting the depth of heat transport and creating a shallow mixed surface layer separated from cooler bottom waters (Herb & Stefan, 2004; Andersen et al., 2017a; Sand-Jensen et al., 2019). In short, macrophytes can induce thermal stratification in small waterbodies, which is frequently observed (Holgerson et al., 2022). Stratification may isolate bottom waters from rising surface temperatures during an aquatic heatwave and is expected to restrict dissolved gas transport, producing a vertically heterogenous chemical environment within macrophyte beds (Andersen et al., 2017b; Vilas et al., 2017). As a result, macrophyte structure could also influence how DO responds to aquatic heatwaves. Rising surface water temperatures during a heatwave are expected to lower DO concentrations; however, in maintaining cooler bottom water temperatures, macrophyte-induced stratification may dampen the effects of a heatwave on gas solubility and DO depletion. Altogether, macrophytes play a key role in the thermal structure and DO environment of small waterbodies, potentially mediating the effect of temporary, external stressors on these ecosystems' structure and function. However, an explicit evaluation of how macrophyte-flow interactions alter ecosystem response to stressors is lacking.

The abundance and growth of macrophytes in small waterbodies is driven by temperature and the availability of light and nutrients (Carpenter & Lodge, 1986; Phillips et al., 2016), making them sensitive to environmental stressors such as nutrient loading and heatwaves (Wu et al., 2021). Warmer water temperatures can enhance macrophyte growth (Olesen & Madsen, 2001; Bertani et al., 2016; Hansson et al., 2020); however, high temperatures may also induce heat stress, impeding reproduction (Li et al., 2017) or prompting senescence (Hao et al., 2018).

Similarly, nutrient loading may have either a positive or negative effect on macrophyte growth. Although macrophytes can benefit from enhanced nutrient availability through foliar uptake (DeMarte & Hartman, 1974; Twilley et al., 1977), nutrient loading can also increase algal biomass and subsequently reduce light availability through shading (Scheffer et al., 1993; Short et al., 1995). The effect of shading from phytoplankton-associated turbidity is expected to vary across macrophyte growth forms, as submersed species are more vulnerable to light limitation than emergent or floating-leaf species (Szabo et al., 2010). While the individual responses of macrophytes to nutrient enrichment and heat stress have been established, it remains unclear how macrophytes respond to simultaneous, compounding stressors and what the consequences are for the thermal and chemical structure of small waterbodies.

We experimentally evaluated the interacting effects of episodic nutrient loading and extreme heat on macrophyte biomass and the subsequent changes in the physicochemical environment in two shallow, vegetated ponds. One of the ponds was pulsed with nutrients to simulate typical storm-driven loading, while the other pond served as a reference. Both ponds experienced a mid-summer heat event following the first experimental nutrient pulse. We hypothesized that the combined stress of the nutrient addition and heat event would induce early senescence of submersed macrophytes, reducing macrophyte biomass and subsequently altering temperature and DO gradients. We asked (Q1) How does macrophyte biomass and canopy height influence pond thermal structure, and does macrophyte presence control vertical heat transfer during a heat event? (Q2) How does spatiotemporal variation in DO relate to macrophyte biomass and canopy height, and does macrophyte presence alter the DO response to a heat event? We evaluated these mechanisms using empirical data and developed a hydrodynamic model of one-dimensional heat transport in vegetated waters. We predicted that greater

macrophyte biomass and canopy height in the reference pond would be associated with stronger thermal stratification and greater differences in DO between surface and bottom waters. We also predicted that macrophyte presence would maintain cooler temperatures and stable DO concentrations during a heat event. Through the combination of our experiment, observations, and modeling, we found that macrophytes structure spatial and seasonal variation in the thermal and chemical environments of shallow waterbodies.

MATERIALS AND METHODS

Study Site and Field Measurements

We studied how macrophyte structure influences spatiotemporal variation in thermal and DO dynamics of small waterbodies in two ponds at Iowa State University's Horticulture Research Station (42.110005, -93.580454) during the summer of 2020. The ponds are rectangular, relatively small (surface area 400 m^2, dimensions 10 m × 40 m; Figure 1), and shallow (2 m maximum depth, 0.8 m mean depth). These waterbodies fit morphometric and functional definitions of ponds (Richardson et al., 2022). The mean depth is below the theoretical threshold distinguishing polymictic from stratifying waterbodies, such that the water column of these ponds is expected to be well-mixed in the absence of internal structure (Kirillin & Shatwell, 2016). Water balance is driven solely from precipitation and evaporation as there are no surface inflows or outflows and the ponds are lined with bentonite to prevent groundwater interactions. As there is effectively no watershed for these ponds, we controlled all external nutrient inputs.

The macrophyte community was composed of longleaf pond weed (*Potamogeton nodosus*; hereafter "floating-leaf") and leafy pondweed (*P. foliosus*; hereafter "submerged"),

158 established from a natural seedbank. The typical phenology of these species follows a pattern of
159 spring emergence from over-wintering structures, growth throughout the summer, and then
160 senescence of the leaves and stems in early autumn. The ponds were initially filled with water
161 from the research station's irrigation reservoir to seed natural phytoplankton and zooplankton
162 communities. There were six total ponds at the site with varying fish communities as a part of a
163 larger experiment (Butts, 2023). Two of the ponds with the same fish community were selected for
164 this study. The ponds were stocked in early spring (15-45 days before measurements began) with
165 yellow perch (*Perca flavescens*) and bluegill (*Lepomis macrochirus*) at roughly 20 kg ha^{-1} for
166 both species, which is within the range of densities for temperate waterbodies (Carlander, 1977;
167 Schneider, 1999).
168 External nutrient loading typical of a discrete storm event in this agricultural region was
169 simulated by adding nitrogen and phosphorus to one of the ponds (hereafter "nutrient addition
170 pond") twice over the course of the summer. Nitrogen as ammonium nitrate (NH_4NO_3), and
171 phosphorus as sodium phosphate monobasic dihydrate ($(NaH_2PO_4 \bullet (H_2O)_2$) in a molar ratio of
172 24N:1P was mixed with pond water in a slurry and then distributed across the surface of the
173 pond. The first nutrient addition (day of year, DOY 176, 24 June 2020) raised the mass of
174 phosphorus in the water column by 3%, and the second addition (DOY 211, 29 July 2020) raised
175 the mass by 5%. These mass increases and stoichiometry are consistent with the expected
176 nutrient loading from a large precipitation event in an agricultural landscape (Vanni et al., 2001;
177 Lürling et al., 2018). Nutrients were not added to the other pond (hereafter "reference pond"). To
178 assess and compare the effects of the nutrient additions on algal biomass, we measured
179 chlorophyll-*a* concentrations daily at the deep site of each pond (Figure 1) using the Total Algae
180 sensor with the YSI ProDSS multiparameter sonde (Yellow Springs Instruments, Yellow
181 Springs, Ohio USA). The sensor logged continuously and was slowly lowered through the water

column. Surface concentrations of chlorophyll-*a* were averaged over 10-30 cm depth. To minimize drift, the sensor was calibrated regularly against laboratory standards. Secchi depth was also measured daily at the same location.

To monitor thermal structure, we deployed vertical strings of high frequency temperature sensors (HOBO 8K Pendant Temperature Data Logger) at three sites, aligned from the deep (2 m) to shallow (1.5 m) ends of each pond (Figure 1). Temperature loggers were distributed throughout the water column every 0.25 m up to 1.5 m and then every 0.5 to the bottom and logged every 30 minutes from May to August (DOY 143-233). We also took high frequency measurements of DO at 0.25 m over the deep site of both ponds (miniDOT Clear Logger; logging every 30 minutes). To quantify the three-dimensional distribution of DO, profiles of DO saturation and water temperature were taken weekly (13 sampling events total) on a grid of 18 sites in each pond (Figure 1). Measurements were taken in the late morning, between 10:00 and 12:00. A continuous profile of DO was logged at each site as the YSI ProDSS multiparameter sonde was slowly lowered through the water column.

We quantified variation in macrophyte structure over space and time by monitoring community composition, canopy height, and biomass from May to August (DOY 143-233). Species presence-absence and canopy height were measured weekly at three sites from the deep to shallow ends of the ponds (Figure 1). Canopy height was measured as the distance from the sediment-water interface to the top of the canopy. Water depth was also measured at these points so that canopy height could be expressed as a proportion of the water column. Macrophyte dry biomass was sampled biweekly (6 sampling events) on the same grid of 18 sites in each pond (Figure 1). Profiles of DO were always taken before biomass was sampled. To collect a biomass sample, a two-side rake was lowered to the bottom and used to remove submersed and floating-

leaf macrophytes from an approximately 0.4 m^2 area (Mikulyuk et al., 2011). The above-sediment tissue was collected from the rake to determine dry biomass by drying the material at 60°C to a constant mass before weighing.

Hydrodynamic Modeling

To explore the mechanisms by which changes in macrophyte biomass and canopy height influence pond thermal structure, we applied a one-dimensional hydrodynamic model for vegetated waterbodies. Our model builds upon the one-dimensional, integral energy model by Herb and Stefan (2004) for heat transport in lakes with submersed macrophytes. Macrophytes are incorporated into the model through two key parameters: a light extinction coefficient due to macrophyte biomass shading and a term for turbulent kinetic energy dissipation by macrophytes based on their surface area and drag. Our contributions to the original model include adding convective overturn to address density instabilities over the diurnal cycles, a dynamic macrophyte growth and senescence boundary condition over time, dynamic light attenuation coefficient for water based on daily Secchi depth, and coding the model in the open-source software R (Appendix S1).

For boundary conditions, the model requires an initial water temperature profile from the temperature chain at the deep site, timeseries of meteorological drivers (air temperature, relative humidity, air pressure, wind speed, and short-wave radiation), and waterbody hypsography (depth-area relationship). We obtained the necessary meteorological data at an hourly timestep from a weather station located approximately 550 meters from the study ponds (ISU Soil Moisture Network, 2021). Macrophyte data were incorporated into the model through weekly measurements of canopy height at the deep site of the reference pond as well as biomass density

(g m^{-3}) measurements taken every two weeks. We used the average biomass density from the two sampling sites closest to the deep site temperature sensors.

The model was run on a 1-hour timestep from late May-August (DOY 143-241; 99 days total). The observed, high frequency water temperature profiles from the deep site of the reference pond were used to calibrate 9 model parameters (Table S1) and assess model fit (quantified as root mean square error, RMSE). Once the model was sufficiently calibrated to the empirical data, we manipulated the input macrophyte data to simulate the effect of different macrophyte biomass and canopy dynamics on thermal structure (Table S2). Specifically, we tested a scenario with no macrophytes present in the pond compared to macrophyte biomass and canopy heights that were measured in the reference pond. All modeling analyses were completed in R version 4.1.2 (R Core Team 2021) using the gotmtools (https://github.com/aemon-j/gotmtools), rLakeAnalyzer (Winslow et al., 2019), lubridate (Garrett & Wickham, 2011), and tidyverse (Wickham et al., 2019) packages.

Statistical Methods

An aquatic heatwave occurs when daily mean surface water temperatures exceed the seasonal 90th percentile of historical measurements for at least 5 days, without dropping below that threshold for two2 or more days (Hobday et al., 2016; Tassone et al., 2021). Since we did not have long-term data on summer water temperatures in the experimental ponds, we elected to use temperature data for the study period only, but a more stringent definition of a heat event threshold (i.e., 95th percentile) for the same extended period (5 days). To determine the 95th percentile of surface water temperature for each pond, we calculated the mean daily temperature from loggers placed at 0 and 0.25 m at the middle at deep sites. A period with at least five days

above the 95th percentile threshold was classified as a sustained aquatic heat event (hereafter, "heat event").

To visualize thermal structure, we used linear interpolation at depths where temperature measurements were missing. Only empirical measurements of water temperature were used in the model and to calculate indices of pond thermal structure (i.e., thermocline depth). Thermocline depth was calculated using the rLakeAnalyzer package. (Winslow et al., 2019). We defined surface water temperature as the average from the 0 and 0.25m sensors. We used the deepest sensors (2m at the middle and deep sites, 1.5m at the shallow sites) for measurements of bottom water temperature. To compare macrophyte biomass between the study ponds, we calculated a weighted average across the 18 sampling sites such that sites around the perimeter of the pond (n=14) had the same weight as sites in the interior or the pond (n=4; Figure 1) so that the mean value would not be biased by water depth.

The vertical distribution of DO saturation was either uniform, highest in the surface waters, or highest in the bottom waters depending on the site and time of year (Figure S1). Therefore, we focused on DO dynamics in the surface and bottom layers by averaging values from 0-0.25 m and the sediment-water interface to 0.25 m above this depth, respectively. To quantify spatial variation within each pond, we calculated the coefficient of variation for DO for each sampling day, standardized by the pond-mean for that day. Temporal variation was calculated based on the coefficient of variation in DO for each sampling site, so variation was due to differences in DO over time, standardized by the summer mean DO saturation for that site. A generalized additive model (GAM) was used to smooth the daily time series of chlorophyll-*a* concentrations and weekly time series of DO saturation to visually highlight differences in trends over time between the nutrient addition and reference pond. All statistical

analyses were completed in R version 4.1.2 (R Core Team 2021) using mgcv (Wood, 2017) in addition to packages used for the hydrodynamic model.

RESULTS

Environmental Stressors and Macrophyte Response

Both ponds experienced a heat event from DOY 185-190 (3-8 July 2020, Figure 2A). During this period, mean daily surface water temperatures exceeded the seasonal 95th percentile in each pond (greater than 29.8 °C in the nutrient addition pond and 30.6 °C in the reference pond). Maximum daily surface water temperatures ranged from 34.5-37.1 °C in the nutrient addition pond and 33.7-38.6 °C in the reference pond during the heat event. Although both ponds had brief periods of high surface water temperatures at other times, DOY 185-190 was the only sustained period of high surface water temperatures ($\geq$ 5 days). The heat event began 9 days after the first nutrient pulse, creating multiple stressors (i.e., eutrophication and prolonged heat stress) for macrophytes in the nutrient addition pond.

At the time of the first nutrient addition (DOY 176), chlorophyll-*a* concentrations were the lowest in the amended pond (Figure 2B). Prior to and during the heat event chlorophyll-*a* concentrations increased in the nutrient addition pond and continued to increase after the second nutrient addition (DOY 211) until the early fall. At that time the reference pond (which did not receive any nutrient input) had higher chlorophyll-*a* concentrations that declined prior to and during the heat event, remaining low until early fall. Heightened chlorophyll-*a* concentrations in the nutrient addition pond are indicative of higher algal biomass and thus phytoplankton-associated turbidity, potentially reducing light availability for submerged macrophytes.

296 Spatiotemporal patterns in macrophyte biomass differed between the ponds and
297 macrophyte growth forms (Figure 2C, 3). The floating-leaf species was largely limited to a ring
298 around the shallower edges of the ponds where the leaves reached the surface. The submerged
299 species was present across a range of depths but reached the highest biomass in the deeper,
300 central region of each pond. In the reference pond, macrophytes followed expected phenology
301 with increasing biomass through to the late summer and then senescence of both growth forms
302 beginning in early autumn (Figure 2C, 3). However, in the nutrient addition pond, submerged
303 macrophytes growing in 1.75 to 2 m of water began to senesce following the initial nutrient
304 addition and heat event such that no plants were present in the deepest areas of the nutrient
305 addition pond nine days (DOY 199) after the heat event and the middle site of the pond 23 days
306 (DOY 213) after the heat event ended (Figure 3). Early senescence of submersed macrophytes in
307 the nutrient addition pond resulted in rapid declines in both biomass (Figure 2C) and canopy
308 height (Figure 4). Both submersed and floating-leaf plants persisted around the shallow edge of
309 the pond through the end of the summer. The temporal mismatch in the senescence of submersed
310 macrophytes between the reference and nutrient addition ponds was qualitatively consistent with
311 the other ponds at the site with differing fish communities, half of which received nutrient
312 additions and the other half were reference ecosystems (Figure S2).
313
314 ***Spatiotemporal Variation in Pond Thermal Structure***
315 Both ponds experienced intermittent thermal stratification and similar spatial patterns of
316 stratification from shallow to deep sites (Figure 4). Early in the summer, both ponds were cool
317 and isothermal. As surface waters warmed, the middle and deep sites of both ponds began to
318 stratify while the shallow sites remained well-mixed. At the center of the reference pond, a stable

thermocline developed between 1-1.5 m from DOY 155-161, and almost constantly between DOY 168-210 (Figure S3A). In the nutrient addition pond, thermocline formation was intermittent (DOY 157-159, 170-174, and 178-192; Figure S3B). When present, thermoclines cooled and deepened slightly (0.05-0.1 m) during the night, indicating nighttime convective cooling and mixing in the surface layer. During periods of thermal stratification, differences between surface and bottom water temperatures ranged from 4.3 to 11.5 °C (mean 8.1°C) in the reference pond and 4.5 to 10.2 °C (mean 7.3 °C) in the nutrient addition pond.

During times of similar macrophyte coverage, either early or late in the season (Figure 4), the thermal structure between the two ponds was similar. For example, both ponds experienced a strong mixing event in late summer (DOY 216-220), driven by cooler air temperatures and higher wind speeds (Figure 5) and facilitated by declining macrophyte structure (Figure 4). Similar meteorological conditions occurred in early summer and resulted in some water cooling (e.g., DOY 164, 175); however, the ponds did not mix as fully during these events, likely due to the macrophyte structure present in both ponds in early summer (Figure 4).

Although the overall seasonal pattern in thermal structure was similar between the ponds, there were brief dissimilarities related to differences in the timing of macrophyte senescence (Figure 4). There was a prolonged period of stable thermal stratification from DOY 180-210 in the reference pond, with only brief instability between DOY 198-199. A stable thermocline set-up in the nutrient addition pond around the same time (DOY 178); however, stratification began to break down approximately 18 days earlier (DOY 192) than in the reference pond (Figure S3). The timing of destratification in the nutrient addition pond coincides with declines in macrophyte biomass (Figure 3) and canopy height (Figure 4) in the center of the pond. Destratification in the reference pond also followed patterns of biomass senescence and loss of canopy height, although

this did not occur until later in the summer in this pond. In both ponds, there was strong temporal coherence between the timing of destratification and macrophyte senescence, with the difference in timing from typical phenology likely spurred by the compounding stress of eutrophication and a heat event in the nutrient addition pond. The declines in canopy cover and biomass were associated with increased thermal mixing and warmer bottom water temperatures, especially in the nutrient addition pond.

During the aquatic heat event (DOY 185-190), both ponds experienced a similar increase in surface water temperatures (Figure 2A, Figure 4). However, there was a stark difference in the response of bottom water temperatures at the deep and middle sites between the ponds (Figure S4). During the heat event, bottom water temperature remained consistent at both the deep and middle sites of the reference pond. The daily mean bottom water temperature increased by only 0.2 °C at both sites. In contrast, bottom water temperatures in the nutrient addition pond increased by 1.3 °C and 1.4 °C at the deep and middle sites, respectively. At the shallow site in both ponds bottom water temperatures increased 1-1.3 °C during the heat event. The different response of bottom water temperature to the heat event related to differences in macrophyte biomass between the two ponds. At the time of the heat event, macrophyte biomass (Figure 2C) and canopy height (Figure 4) were greater in the reference pond as submersed macrophytes in the center of the nutrient addition pond had begun to senesce (Figure 3). Overall, bottom waters in the nutrient addition pond warmed during the heat event while cooler temperatures were maintained in the reference pond, despite significant warming in the surface layers.

Spatiotemporal Variation in Dissolved Oxygen

In both ponds, DO varied across sites, vertically in the water column, and over time. Weekly DO profiles captured broad seasonal trends in surface DO saturation as similar temporal patterns were observed between weekly and high-frequency values (Figure 2D, S5A). Early in the summer, both ponds were supersaturated in DO in the surface waters (Figure 2D), and mean surface saturation was similar between the ponds before the initial nutrient addition. In the reference pond, DO remained stable until the heat event (DOY 185-190), after which saturation declined and generally remained below saturation for the remainder of the study period. In contrast, mean surface DO saturation in the nutrient addition pond declined immediately following the first nutrient addition (DOY 176) and remained below saturation for the rest of the summer. Over a one-week period during and after the heat event (DOY 186-192), DO saturation fell 22.4% and 50.4% in the nutrient addition and reference ponds, respectively. Bottom water DO saturation mirrored the seasonal pattern in surface DO (Figure S5B). For both ponds the difference in DO saturation between surface and bottom waters was most pronounced early in the season (reference pond range of difference from -87.1 to 23.3%; nutrient addition pond range -56.8 to 58.8%). Surface and bottom water DO saturation became more similar throughout the summer, especially following the heat event (reference pond range of difference -2.1 to 17.0%; nutrient addition pond range -0.3 to 12.2%; Figure S5C).

For both surface and bottom water DO saturation, temporal variation on a seasonal scale was greater than spatial variation within the ponds (Table 1). The coefficient of variation at a given site in the pond over time was 3.6-5.2 times greater than the variation among sites on a given sampling day. The magnitude of temporal versus spatial variation was similar between ponds. Seasonal patterns in DO saturation followed some trends with declining macrophyte

biomass, with lower DO following the nutrient addition; however, the heat event had the most pronounced effect on seasonal DO saturation (Figure 6).

Mechanisms of Macrophyte Control of Pond Hydrodynamics

We used a one-dimensional hydrodynamic model to illuminate the mechanistic relationship between macrophytes and pond thermal structure and test how macrophyte presence mediates the degree to which bottom water temperatures warm in response to a heat event. We based our model on the deep site of the reference pond. The model projections were consistent with the observed temperature profiles (mean RMSE 1.67 °C across 8 discrete depths; Figure S6). Error was greatest in the surface waters (0 m; RMSE 2.47 °C), where the model underpredicted water temperature and did not capture the full range of observed diel oscillations, especially early in the summer. Error was lower in the bottom waters of the pond (1.25-2 m) where the model underpredicted water temperature early in the summer but then showed good agreement with the observed temperatures (RMSE range 1.05-1.52 °C). Overall, the model captured the magnitude and seasonal trends of temperature throughout the water column.

We applied the hydrodynamic model to quantify differences in pond thermal structure under contrasting scenarios of macrophyte presence (Figure 7). Specifically, we tested a scenario in which there were no macrophytes present (i.e., canopy height and biomass density were set to zero over the study period) and compared the results to the model output for the reference pond when the observed macrophyte data were used (Table S2). Under the scenario where macrophytes were present, the model predicted strong stratification during the period of peak macrophyte biomass and canopy height in the middle of the summer and cool bottom water temperatures throughout the study period (Figure 7A). In contrast, under the scenario in which

409 macrophytes were entirely absent from the pond, the model predicted complete water column
410 mixing and much warmer temperatures throughout the water column, especially following the
411 aquatic heat event (Figure 7B). This is consistent with the prediction of polymixis for these
412 ponds based on bathymetry (Kirillin & Shatwell, 2016). When macrophytes were present, the
413 increase in bottom water temperatures in the simulation over the course of the aquatic heat event
414 was negligible (0.01 °C), and bottom temperatures remained below 25 °C for the remainder of
415 the summer (maximum temperature 23.3 °C; Figure 7A, C). However, in the no-macrophyte
416 scenario bottom water temperatures increased by 1.92 °C during the heat event and had much
417 higher maximum water temperatures later in the summer (33.4 °C; Figure 7B, C). The model
418 simulations demonstrate that macrophyte structure increases thermal stratification and promotes
419 cooler bottom water temperatures, even during an extreme heat event.
420
421 **DISCUSSION**
422 We applied an ecosystem experiment and complimentary hydrodynamic model to test
423 macrophyte response to compounding stressors (i.e., stochastic external nutrient loading and an
424 extreme heat event) and evaluate the consequences for the physicochemical environment in two
425 shallow, vegetated ponds. The type and severity of environmental stressors differed between the
426 study ponds, producing distinct seasonal trajectories in macrophyte assembly and coverage. In
427 the reference pond, both submersed and floating-leaf macrophytes followed the expected
428 phenology of spring emergence, summer growth, and then senescence beginning in late summer.
429 This natural phenology may be attributed to the lack of severe physiological stressors in the
430 reference pond. Although this pond did experience a sustained heat event, dense macrophyte
431 beds limited the depth of water column warming and maintained stable bottom water

temperatures. In contrast, submersed macrophytes in the nutrient addition pond began to senesce in mid-summer after the first experimental nutrient pulse and continuing after the heat event. This early senescence was limited to submersed macrophytes in the deeper, central region of the pond, suggesting that light limitation from phytoplankton shading may have been a contributing stressor (Scheffer et al., 1993; Short et al., 1995; Phillips et al., 2016). Unlike the reference pond, chlorophyll-*a* concentrations continued to rise in the nutrient addition pond, maintaining any light limitation stress. The combination of some light limitation with more acute heat stress due to higher bottom temperatures during the heat event may have been the catalyst for the observed early senescence trajectory in the nutrient addition pond. Qualitatively, the same declining trajectory in macrophyte biomass was observed in the other ponds on site that received nutrient additions but had higher resilience to the nutrient pulses (Butts, 2023), supporting our hypothesis that the combined stressors of eutrophication and intense heat led to the early decline. Regardless of the driver, the observed early senescence of submersed macrophytes in the nutrient addition pond altered the thermal environment and DO saturation in relation to the reference pond.

Thermal Structure

On a seasonal scale, we observed strong temporal coherence between macrophyte growth and senescence and pond thermal structure. Both ponds experienced intermittent thermal stratification in early summer, once macrophytes had grown to fill most of the water column. This threshold is consistent with the expectation that canopy-forming macrophyte beds may induce diurnal stratification once they occupy at least 50% of the water column (Vilas et al., 2017) as well as observed stratification in many small waterbodies (Holgerson et al., 2022). By mid-summer we observed strong thermal stratification, characterized by large differences

(around 10°C) between surface and bottom water temperatures, comparable to stratification reported in other small, vegetated ponds (Andersen et al., 2017a; Vilas et al., 2017). However, in other studies, macrophyte-induced stratification followed diel cycles, with daytime stratification and nighttime overturn due to convective mixing (Martinsen et al., 2019; Sand-Jensen et al., 2019), which can move through macrophyte structure more readily than external turbulent mixing (Herb & Stefan, 2005; Andersen et al., 2017b). Although we observed nighttime convective cooling and mixing in the surface of the ponds during periods of macrophyte-induced stratification, convective cooling did not mix the entire water column. Stable thermal stratification began to break down in both study ponds during macrophyte senescence, the timing of which varied between ponds. Declining macrophyte canopy height and biomass removed structural barriers that had previously attenuated incoming solar radiation and dissipated wind-driven turbulent mixing (Herb & Stefan, 2004), allowing the warm, mixed surface layer to deepen and eventually mix the entire water column.

Macrophyte presence mediated how pond thermal structure responded to a sustained heat event by restricting vertical heat transfer and maintaining cooler bottom water temperatures. Both study ponds saw high surface water temperatures during the heat event. However, as anticipated, the depth of water column warming and change in bottom water temperature differed between the reference and nutrient addition ponds (+0.2°C vs. 1.3°C, respectively) due to differences in macrophyte coverage and canopy height (75% of the water column vs. 0%, respectively). Macrophyte structure clearly played a pivotal role in mediating the depth and degree of water column warming during the aquatic heat event. Nevertheless, thermal structure in small waterbodies arises from complex interactions between waterbody features and external forces (Herb & Stefan, 2004; Branco & Torgersen, 2009, Holgerson et al., 2022). To explicitly

test the mechanisms underpinning the differences we observed between the study ponds, we used a hydrodynamic model for heat transport in vegetated waterbodies and simulated water column thermal structure during a heat event under contrasting scenarios of macrophyte density.

The model results support our field observations and demonstrate that macrophytes structure the thermal environment in shallow ponds through vertical attenuation of both light and turbulent kinetic energy. Simulations of seasonal patterns in pond thermal structure under variable macrophyte density revealed that macrophyte presence reduces the depth and degree of water column warming both during and after an aquatic heat event and maintains cooler bottom water temperatures throughout the course of the summer. Our experimental observations and model simulations provide evidence that macrophytes can buffer small waterbodies from brief aquatic heatwaves, particularly the vertical extent of warming in the water column. As aquatic heatwaves become more widespread and frequent, heatwaves in small waterbodies are expected to be shorter but more intense compared to larger waters (i.e., due to lower thermal inertia; Woolway et al., 2021a; Polazzo et al., 2021; Woolway et al., 2022). Our findings suggest that macrophytes can mediate the intensity of brief aquatic heatwaves in small lakes and ponds. As such, managing for robust macrophyte communities is a potential tool for mitigating heatwave effects in small waterbodies and promoting thermal habitat refugia to support other aquatic organisms (Carpenter & Lodge, 1986; Till et al., 2019).

Our hydrodynamic model enhances a conceptual and analytical framework for incorporating biological structure into one-dimensional heat transport models (Herb & Stefan, 2004). Overall, there was good agreement between the model predictions and observed temperature profiles. The largest discrepancies between the model output and field data occurred in early summer when the model underpredicted temperature. The early summer period

coincides with rapid growth in macrophyte biomass and canopy height. It is possible that the temporal resolution of our weekly canopy height measurements and biweekly biomass collections was insufficient to accurately capture biological dynamics in the pond for the model input. There was also a one-day period of high air temperatures (DOY 155) early in the summer that caused a rapid change in water temperature. Other one-dimensional heat transport models (i.e., Simstrat; General Ocean Turbulence Model, GOTM; General Lake Model, GLM) have greater error during extreme meteorological events, including atmospheric heatwaves (Mesman et al., 2020), which may be the case with our model as well during this early-season, rapid warm-up. Our model would benefit from additional testing across a variety of vegetated waterbodies to inform best practices for applying this approach in other waters. However, our findings support the need to incorporate vegetation dynamics into hydrodynamic models, and our modeling approach provides an example of how to do so.

Dissolved Oxygen

There was little spatial variability in DO saturation, contrary to observations in other vegetated waterbodies (Andersen et al., 2017a; Vilas et al., 2017). Most of the DO profiles were uniform with depth, suggesting that the balance of processes releasing and consuming oxygen (e.g., gross primary production versus respiration) were similar throughout the ponds or that DO was able to readily equilibrate. Temporal variation in surface and bottom water DO saturation were connected to the compounding environmental stressors, beginning with the initial experimental nutrient addition. Following the first nutrient pulse, DO remained stable in the reference pond but declined below 100% saturation in the experimental pond. The observed decline in DO suggests that ecosystem respiration was stimulated by the added nutrients,

524 outweighing any increases in gross primary production. Stress-induced macrophyte senescence
525 likely contributed to this pattern through reduced macrophyte photosynthesis and increased
526 macrophyte decomposition. Although we observed differences in DO saturation between the
527 ponds after the nutrient addition, the most pronounced temporal shift in DO occurred following
528 the heat event.

529 During the heat event, DO saturation fell sharply in both ponds and remained depressed
530 through the remainder of the study period. We had expected macrophyte structure to maintain
531 stable DO saturation in the bottom waters of the reference pond; however, both ponds responded
532 similarly, regardless of the differences in macrophyte coverage and thermal structure. In addition
533 to lower oxygen solubility in warmer water, organic carbon mineralization in sediments is
534 strongly controlled by temperature (Gudasz et al., 2010; Cardosa et al., 2014) and the heat event
535 likely spurred microbial respiration, which has been observed during heatwaves in both
536 freshwater and marine ecosystems. (Ali et al., 2016; Brauko et al., 2020; Tassone et al., 2021).
537 Reduced DO availability has consequences for nutrient and carbon cycling as well as greenhouse
538 gas production. For example, anoxia within the sediment profile can mobilize phosphorus from
539 redox-sensitive minerals (Orihel et al., 2017). Anoxic conditions and increased organic matter
540 availability (e.g., from macrophyte necromass) also promote denitrification and methanogenesis,
541 two microbial processes that produce potent greenhouse gases (Bastviken et al., 2005; Fonseca et
542 al., 2017; Ming et al., 2022). Although both ponds likely experienced shifts in other elemental
543 cycles as a result of reduced DO saturation during the aquatic heat event, the consequences for
544 greenhouse gas production were likely more pronounced in the nutrient addition pond due to
545 early macrophyte senescence increasing organic matter inputs to the sediments. This difference

between the study ponds highlights the complex interactions that may arise from compounding stressors in lentic ecosystems.

Conclusions

Aquatic heatwaves are becoming more frequent and are likely to co-occur with chlorophyll-*a* maxima in lakes and ponds (i.e., algal blooms; Woolway et al., 2021b). As such, there is a growing need to understand how lentic ecosystems will respond to compound, extreme events to inform water resource and biodiversity management. Our findings illuminate the role that macrophyte-hydrodynamic interactions play in mediating aquatic ecosystem response to multiple stressors. Overall, dense macrophyte structure can buffer small waterbodies from brief aquatic heat events by restricting vertical heat transport. However, declines in DO saturation are expected during heat events, regardless of macrophyte coverage. Our findings also reinforce that macrophyte communities in small lakes and ponds are vulnerable to nutrient loading and temperature extremes. Given the prevalence and importance of small waterbodies for biodiversity and biogeochemical processing, it is essential that we continue to build our mechanistic understanding of the effects of compound, extreme events in these ecosystems and the role that macrophytes can play in ameliorating stressors.

Acknowledgements

Albright was supported by the National Science Foundation (NSF) Graduate Research Fellowship Program (DGE-1747503). Additional Support was also provided by the Graduate School and the Office of the Vice Chancellor for Research and Graduate Education at the University of Wisconsin-Madison with funding from the Wisconsin Alumni Research

Foundation. Wilkinson was supported by the NSF Division of Environmental Biology (1942256 and 2200391). Ladwig was supported by the NSF Harnessing the Data Revolution grant (1934633), the University of Wisconsin-Madison Data Science Initiative, and the NSF Advances in Biological Informatics development grant (DBI 1759865). Any opinions, findings, and conclusions or recommendations expressed in this material are those of the authors and do not necessarily reflect the views of the National Science Foundation. Thank you to Tyler Butts, Matthew Kots, Michael Tarnow, and Robert Johnson for collection and use of ancillary data sets.

Author Contributions

Ellen Albright and Grace Wilkinson designed the study. Ellen Albright collected and analyzed the field data. Robert Ladwig and Ellen Albright designed and ran the hydrodynamic model. Ellen Albright wrote the first draft. Grace Wilkinson provided substantial feedback on the first draft. All authors assisted with later revisions.

Data Availability Statement

The data supporting the conclusions and the analysis code are available in the Github repository https://github.com/AlbrightE/pond_physics_2022. Following manuscript acceptance, the Github repository will be archived on Zenodo, and the data will be published on the Environmental Data Initiative's online repository under a Creative Commons Attribution license (CC-BY).

REFERENCES

Ali, S., P.K. Mishra, A. Islam, and N.M. Alam. 2016. Simulation of water temperature in a small pond using parametric statistical models: Implications of climate warming. J. Environ. Eng. 143(3): 04015085, https://doi.org/10.1061/(ASCE)EE.1943-7870.0001050

Andersen, M.R., T. Kragh, and K. Sand-Jensen. 2017a. Extreme diel dissolved oxygen and carbon cycles in shallow vegetated lakes. Proc. Biol. Sci. 284: 20171427, https://doi.org/10.1098/rspb.2017.1427

Andersen, M.R., K. Sand-Jensen, R.I. Woolway, I.D. and Jones. 2017b. Profound daily vertical stratification and mixing in a small, shallow, wind-exposed lake with submerged macrophytes. Aquat. Sci. 79: 395-406, https://doi.org/10.1007/s00027-016-0505-0

Bastviken, S.K., P.G. Eriksson, A. Premrov, and K. Tonderski. 2005. Potential denitrification in wetland sediments with different plant species detritus. Ecol. Eng. 24(2): 183-190, https://doi.org/10.1016/j.ecoleng.2005.04.013

Battin, T. J., S. Luyssaert, L.A. Kaplan, A.K. Aufdenkampe, A. Richter, and L.J. Tranvik. 2009. The boundless carbon cycle. Nat. Geosci. 2: 598-600, https://doi.org/10.1038/ngeo618

Bertani, I., R. Primicerio., and G. Rossetti. 2016. Extreme climatic event triggers a lake regime shift that propagates across multiple trophic levels. Ecosystems. 19(1): 16–31, https://doi.org/10.1007/s10021-015-9914-5

Biggs, J., S. von Fumetti, and M. Kelly-Quinn. 2017. The importance of small waterbodies for biodiversity and ecosystem services: implications for policy makers. Hydrobiologia. 793: 3-39, https://doi.org/10.1007/s10750-016-3007-0

Borchers, H.W. 2021. adagio: Discrete and Global Optimization Routines. R package version 0.8.4. https://CRAN.R-project.org/package=adagio

Branco, B.F., and T. Torgersen. 2009. Predicting the onset of thermal stratification in shallow inland waterbodies. 71(1): 65-79, https://doi.org/10.1007/s00027-009-8063-3

Brauko, K.M., and others. 2020. Marine Heatwaves, Sewage and Eutrophication Combine to Trigger Deoxygenation and Biodiversity Loss: A SW Atlantic Case Study. Front. Mar. Sci. 7, https://doi.org/10.3389/fmars.2020.590258

Butts, Tyler J. "Investigating Ecosystem-Scale Responses to Changes in Lake Food Webs." Order No. 30492440 The University of Wisconsin - Madison, 2023. United States -- Wisconsin: ProQuest. Web. 16 June 2023.

Cardoso, S.J., A. Enrich-Prast, M.L. Pace, and F. Roland. 2014. Do models of organic carbon mineralization extrapolate to warmer tropical sediments? Limnol. Oceanogr. 59(1): 48-54, https://doi.org/10.4319/lo.2014.59.1.0048

623 Carlander, K.D. 1977. Biomass, Production, and Yields of Walleye (Stizostedion vitreum
624 vitreum) and Yellow Perch (Perca flavescens) in North American Lakes. J. Fish. Res.
625 Board Can. 34(10): 1602-1612, https://doi.org/10.1139/f77-225

626 Carpenter, S.R., and D.M. Lodge. 1986. Effects of submersed macrophytes on ecosystem
627 processes. Aquat. Bot. 26: 341-370, https://doi.org/10.1016/0304-3770(86)90031-8

628 Cole, J.J., and others. 2007. Plumbing the global carbon cycle: Integrating inland waters into the
629 terrestrial carbon budget. Ecosystems. 10(1): 171-184, https://doi.org/10.1007/s10021-006-
630 9013-8

631 DeMarte, J.A., and R.T. Hartman. 1974. Studies of Absorption of ^{32}P, ^{59}Fe, and ^{45}Ca by Water-
632 Milfoil (Myriophyllum Exalbescens Fernald). Ecology, 55(1): 188-194,
633 https://doi.org/10.2307/1934635

634 Downing, J. 2010. Emerging global role of small lakes and ponds: little things mean a lot.
635 Limnetica. 29(10): 9-24.

636 Fonseca, A.L.D., C.C. Marinho, and F.D. Esteves. 2017. Potential methane production
637 associated with aquatic macrophytes detritus in a tropical coastal lagoon. Wetlands. 37(4):
638 763-771, https://doi.org/10.1007/s13157-017-0912-6

639 Gudasz, C., D. Bastviken, K. Steger, K. Premke, S. Sobek, and L.J. Tranvik. 2010. Temperature-
640 controlled organic carbon mineralization in lake sediments. Nature. 466: 478–481,
641 https://doi.org/10.1038/nature09186

642 Hao, B., A.F. Roejkjaer, H. Wu, Y. Cao, E. Jeppesen, and W. Li. 2018. Responses of primary
643 producers in shallow lakes to elevated temperature: a mesocosm experiment during the
644 growing season of Potamogeton crispus. Aquat. Sci. 80: 34,
645 https://doi.org/10.1007/s00027-018-0585-0

646 Hansson, L.-A., M.K. Ekvall., L. He, Z. Li, M. Svensson, P. Urrutia-Cordero, and H. Zhang.
647 2020. Different climate scenarios alter dominance patterns among aquatic primary
648 producers in temperate systems. Limnol. Oceanogr. 65(10): 2328–2336,
649 https://doi.org/10.1002/lno.11455

650 Herb, W.R., and H.G. Stefan. 2004. Temperature stratification and mixing dynamics in a shallow
651 lake with submersed macrophytes. Lake Reserv. Manag. 20(4): 296-308,
652 https://doi.org/10.1080/07438140409354159

653 Herb, W.R., and H.G. Stefan. 2005. Model for Wind-Driven Vertical Mixing in a Shallow Lake
654 with Submersed Macrophytes. J. Hydraul. Eng. 131(6): 488-496,
655 https://doi.org/10.1061/(ASCE)0733-9429(2005)131:6(488)

656 Hobday, A.J., and others. 2016. A hierarchical approach to defining marine heatwaves. Prog.
657 Oceanogr. 141: 227-238, https://doi.org/10.1016/j.pocean.2015.12.014

Holgerson, M.A., and P. A. Raymond. 2016. Large contribution to inland water CO_2 and CH_4 emissions from very small ponds. Nat. Geosci. 9: 222-226, https://doi.org/10.1038/ngeo2654

Holgerson, M.A., and others. 2022. Classifying mixing regimes in ponds and shallow lakes. Water Resources Research, 58: e2022WR032522. https://doi.org/10.1029/2022WR032522

Hughes, T.P., and others. 2017. Global warming and recurrent mass bleaching of corals. Nature. 543: 373-377, https://doi.org/10.1038/nature21707

Iowa Environmental Mesonet. 2020. Iowa State University Soil Moisture Network. https://mesonet.agron.iastate.edu/agclimate/hist/hourly.php. Accessed 15 November 2021.

Kirillin, G., and T. Shatwell. 2016. Generalized scaling of seasonal thermal stratification in lakes. Earth Sci. Rev. 161: 179-190, https://doi.org/10.1016/j.earscirev.2016.08.008

Li, Z., L. He, H. Zhang, P. Urrutia-Cordero, M.K. Ekvall, J. Hollander, and L.-A. Hansson. 2017. Climate warming and heat waves affect reproductive strategies and interactions between submerged macrophytes. Glob. Chang. Biol. 23: 108–116, https://doi.org/10.1111/gcb.13405

Licci, S., H. Nepf, C. Delolme, P. Marmonier, T.J. Bouma, and S. Puijalon. 2019. The role of patch size in ecosystem engineering capacity: a case study of aquatic vegetation. Aquat. Sci. 81(3), https://doi.org/10.1007/s00027-019-0635-2

Lürling, M., M. M. Mello, F. van Oosterhout, L. de S. Domis, and M. M. Marinho. 2018. Response of natural cyanobacteria and algae assemblages to a nutrient pulse and elevated temperature. Front. Microbiol. 9: 1–14, https://doi.org/10.3389/fmicb.2018.01851

Martinsen, K.T., M.R. Andersen, and K. Sand-Jensen. 2019. Water temperature dynamics and the prevalence of daytime stratification in small temperate shallow lakes. Hydrobiologia. 826: 247–262, https://doi.org/10.1007/s10750-018-3737-2

Mesman, J.P., and others. 2020. Performance of one-dimensional hydrodynamic lake models during short-term extreme weather events. Environ. Modell. Softw. 133: 104852, https://doi.org/10.1016/j.envsoft.2020.104852

Messager, M.L., B. Lehner, G. Grill, I. Nedeva, and O. Schmitt. 2016. Estimating the volume and age of water stored in global lakes using a geo-statistical approach. Nat. Comm., 7: 13603, https://doi.org/10.1038/ncomms13603

Ming, N., X. Liang, L.J. Hou, W.P. Li, and C.Q. He. 2022. Submerged macrophytes regulate diurnal nitrous oxide emissions from a shallow eutrophic lake: A case study of Lake Wuliangsuhai in the temperate arid region of China. Sci. Total. Environ. 811: 152451, https://doi.org/10.1016/j.scitotenv.2021.152451

Olesen, B., and T.V. Madsen. 2001. Growth and physiological acclimation to temperature and inorganic carbon availability by two submerged aquatic macrophyte species, Callitriche

cophocarpa and Elodea canadensis. Funct. Ecol. 14(2): 252-260, https://doi.org/10.1046/j.1365-2435.2000.00412.x

Oliver, E.C.J., and others. 2018. Longer and more frequent marine heatwaves over the past century. Nat. Commun. 9, 1324, https://doi.org/10.1038/s41467-018-03732-9

Orihel, D.M., H.M. Baulch, N.J. Casson, R.L. North, C.T. Parsons, D.C.M Seckar, and J.J. Venkiteswaran. 2017. Internal phosphorus loading in Canadian fresh waters: a critical review and data analysis. Can. J. Fish. Aquat. Sci. 74: 2005-2029, https://doi.org/10.1139/cjfas-2016-0500

Peacock, M., and others. 2021. Small artificial waterbodies are widespread and persistent emitters of methane and carbon dioxide. Glob. Chang. Biol. 27(20): 5109-5123, https://doi.org/10.1111/gcb.15762

Phillips, G., N. Willby, and B. Moss. 2016. Submerged macrophyte decline in shallow lakes: What have we learnt in the last forty years? Aquat. Bot. 135: 37-45, https://doi.org/10.1016/j.aquabot.2016.04.004

Polazzo, F., S.K. Roth, M. Hermann, A. Mangold-Döring, A. Rico, A. Sobek, P.J. Van den Brink, M.C. Jackson. 2022. Combined effects of heatwaves and micropollutants on freshwater ecosystems: Towards an integrated assessment of extreme events in multiple stressors research. Glob. Chang. Biol. 28: 1248-1267, https://doi.org/10.1111/gcb.15971

Richardson, D.C., and others. 2022. A functional definition to distinguish ponds from lakes and wetlands. Sci. Rep. 12: 10472, https://doi.org/10.1038/s41598-022-14569-0

Sand-Jensen, K., M.R. Andersen, K.T. Martinsen, J. Borum, E. Kristensen, and T. Kragh. 2019. Shallow plant-dominated lakes – extreme environmental variability, carbon cycling and ecological species challenges. Ann. Bot. 124: 35-366. https://doi.org/10.1093/aob/mcz084

Scheffer, M., and others. 2006. Small habitat size and isolation can promote species richness: second-order effects on biodiversity in shallow lakes and ponds. Oikos. 112(1): 227-231, https://doi.org/10.1111/j.0030-1299.2006.14145.x

Scheffer, M., S.H. Hosper, M.L. Meijer, B. Moss, and E. Jeppesen. 1993. Alternative equilibria in shallow lakes. Trends. Ecol. Evol. 8 (8): 275-279, https://doi.org/10.1016/0169-5347(93)90254-M

Schneider, J.C. 1999. Dynamics of quality bluegill populations in two Michigan lakes with dense vegetation. N. Am. J. Fish. Manage. 19(1): 97-109, https://doi.org/10.1577/1548-8675(1999)019<0097:DOQBPI>2.0.CO;2

Short, F.T., D.M. Burdick, and J.E. Kaldy III. 1995. Mesocosm experiments quantify the effects of eutrophication on eelgrass, Zostera marina. Limnol. Oceanogr. 40(4): 740-749, https://doi.org/10.4319/lo.1995.40.4.0740

729 Strydom, S., and others. 2020. Too hot to handle: Unprecedented seagrass death driven by
730 marine heatwave in a World Heritage Area. Glob. Change. Biol. 26(6): 3525-3538,
731 https://doi.org/10.1111/gcb.15065

732 Szabo, S., M. Scheffer, R. Roijackers, B. Waluto, M. Braun, P.T. Nagy, G. Borics, and L.
733 Zambrano. 2010. Strong growth limitation of a floating plant (Lemna gibba) by the
734 submerged macrophyte (Elodea nuttallii) under laboratory conditions. Freshwater. Biol.
735 55(3): 681-690, https://doi.org/10.1111/j.1365-2427.2009.02308.x

736 Tassone, S.J., A.F. Besterman, C.D. Buelo, J.A. Walter, and M.L. Pace. 2021. Co-occurrence of
737 aquatic heatwaves with atmospheric heatwaves, low dissolved oxygen, and low pH events
738 in estuarine ecosystems. Estuar. Coast. 45: 707-720, https://doi.org/10.1007/s12237-021-
739 01009-x

740 Taylor, S., P.J. Gilbert, D.A. Cooke, M.E. Deary, and M.J. Jeffries. 2019. High carbon burial
741 rates by small ponds in the landscape. Front. Ecol. Environ. 17(1): 25-31,
742 https://doi.org/10.1002/fee.1988

743 Till, A., A.L. Rypel, A. Bray, and S.B. Fey. 2019. Fish die-offs are concurrent with thermal
744 extremes in north temperate lakes. Nat. Clim. Chang. 9, 637–641,
745 https://doi.org/10.1038/s41558-019-0520-y

746 Twilley, R.R., M.M., Brinson, and G.J. Davis. 1977. Phosphorus absorption, translocation, and
747 secretion in Nuphar luteum. Limnol. Oceanogr. 22(6): 1022-1032,
748 https://doi.org/10.4319/lo.1977.22.6.1022

749 Van Geest, G.J., F.C.J.M. Roozen, H. Coops, R.M.M. Roijackers, A.D. Buijse, E.T.H.M.
750 Peeters, and M. Scheffer. 2003. Vegetation abundance in lowland flood plan lakes
751 determined by surface area, age and connectivity. Freshw. Biol. 48(3): 440-454,
752 https://doi.org/10.1046/j.1365-2427.2003.01022.x

753 Vanni, M. J., W. H. Renwick, J. L. Headworth, J. D. Auch, and M. H. Schaus. 2001. Dissolved
754 and particulate nutrient flux from three adjacent agricultural watersheds: A five-year study.
755 Biogeochemistry 54: 85–114, https://doi.org/10.1023/A:1010681229460

756 Vilas, M.P, C.L. Marti, M.P. Adams, C.E. Oldham, and M.R. Hipsey. 2017. Invasive
757 macrophytes control the spatial and temporal patterns of temperature and dissolved oxygen
758 in a shallow lake: A proposed feedback mechanism of macrophyte loss. Front. Plant. Sci. 8:
759 2097. https://doi.org/10.3389/fpls.2017.02097

760 Wilkinson, G.M., A. Besterman, C. Buelo, J. Gephart, and M.L. Pace. 2018. A synthesis of
761 modern organic carbon accumulation rates in coastal and aquatic inland ecosystems. Sci.
762 Rep. 8: 15736, https://doi.org/10.1038/s41598-018-34126-y

763 Williams, P., M. Whitfield, J. Biggs, S. Bray, G. Fox, P. Nicolet, and D. Sear. 2004.
764 Comparative biodiversity of rivers, streams, ditches and ponds in an agricultural landscape

765 in Southern England. Biol. Conserv. 115(2): 329-341, https://doi.org/10.1016/S0006-
766 3207(03)00153-8

767 Wernberg, T., and others. 2016. Climate-driven regime shift of a temperate marine ecosystem.
768 Science. 353(6295): 169-172, https://doi.org/10.1126/science.aad8745

769 Woolway, R. I., E. Jennings, T. Shatwell, M. Golub, D.C. Pierson, and S.C. Maberly. 2021a.
770 Lake heatwaves under climate change. Nature. 589: 402-407,
771 https://doi.org/10.1038/s41586-020-03119-1

772 Woolway, R.I., B.M. Kraemer, J. Zscheischler, and C. Albergel. 2021b. Compound hot
773 temperature and high chlorophyll extreme events in global lakes. Environ. Res. Lett.
774 16(12): 124066, https://doi.org/10.1088/1748-9326/ac3d5a

775 Woolway, R.I., C. Albergel, T.L. Frölicher, and M. Perroud. 2022. Severe Lake Heatwaves
776 Attributable to Human-Induced Global Warming. Geophys. Res. Lett. 49(4):
777 e2021GL097031, https://doi.org/10.1029/2021GL097031

778 Wu, H., B. Hao, H. Jo, Y. Cai. 2021. Seasonality and species specificity of submerged
779 macrophyte biomass in shallow lakes under the influence of climate warming and
780 eutrophication. Front. Plant Sci. 12: 678259, https://doi.org/10.3389/fpls.2021.678259

781

TABLES

Table 1. *Temporal versus spatial variation in DO saturation*

		Temporal Variation in DO Saturation		***Spatial Variation in DO Saturation***	
Layer	*Pond*	*CV (%)* Mean	*CV (%)* Range	*CV (%)* Mean	*CV (%)* Range
Surface	Reference	28.9	20.2 – 34.4	5.9	1.8 – 11.3
	Nutrient Addition	22.8	20.6 – 28.8	4.4	2.1 – 9.5
Bottom	Reference	34.4	24.1 – 45.6	7.5	2.0 – 16.3
	Nutrient Addition	26.8	22.1 – 40.3	7.5	2.0 – 16.9

FIGURES

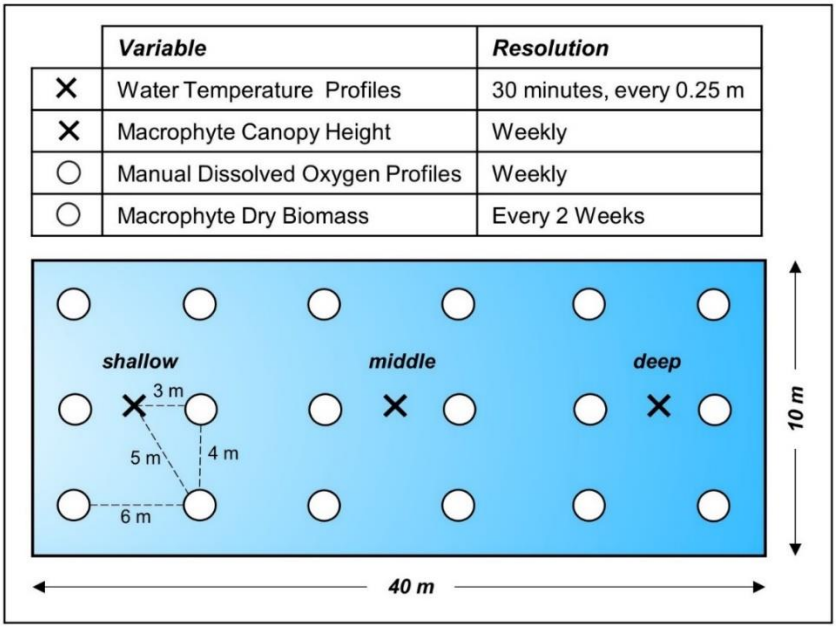

Figure 1. Spatial and temporal resolution of measured variables and sample site locations.

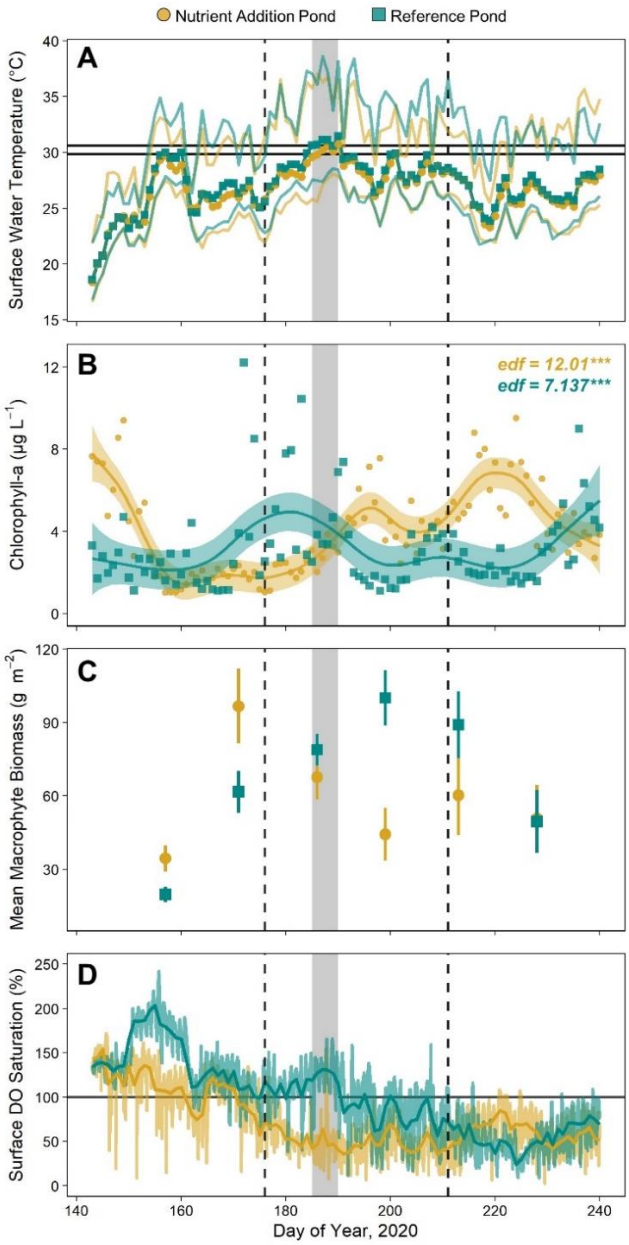

788
789 **Figure 2.** (A) Timeseries of daily surface (0-0.25 m) water temperature. Points represent daily
790 means while lighter lines above and below mark daily maximum and minimum temperatures.
791 Surface sensors at the deep and middle sites were used for pond averages. The 95th percentile
792 surface water temperature thresholds are noted in horizontal lines for the nutrient addition
793 (29.8°C) and reference (30.6°C) ponds. (B) Timeseries of surface (0.1-0.3 m) chlorophyll-*a*
794 concentrations. Values from each pond were GAM-fit to highlight temporal trends. The asterisks
795 next to the effective degrees of freedom (edf) correspond to the estimated p-value, with ***
796 denoting $p < 0.001$. (C) Time series of mean macrophyte biomass in each pond. Error bars mark
797 the standard error of the mean. (D) High frequency surface (0.25 m) dissolved oxygen (DO)
798 saturation at the deep site of each pond over the study period. The daily mean is plotted in a
799 darker line. The horizontal grey line marks 100% saturation. Across all panels, dashed lines mark
800 the timing of nutrient additions (DOY 176, 211) and the grey box highlights the aquatic heat
801 event (DOY 185-190).

802

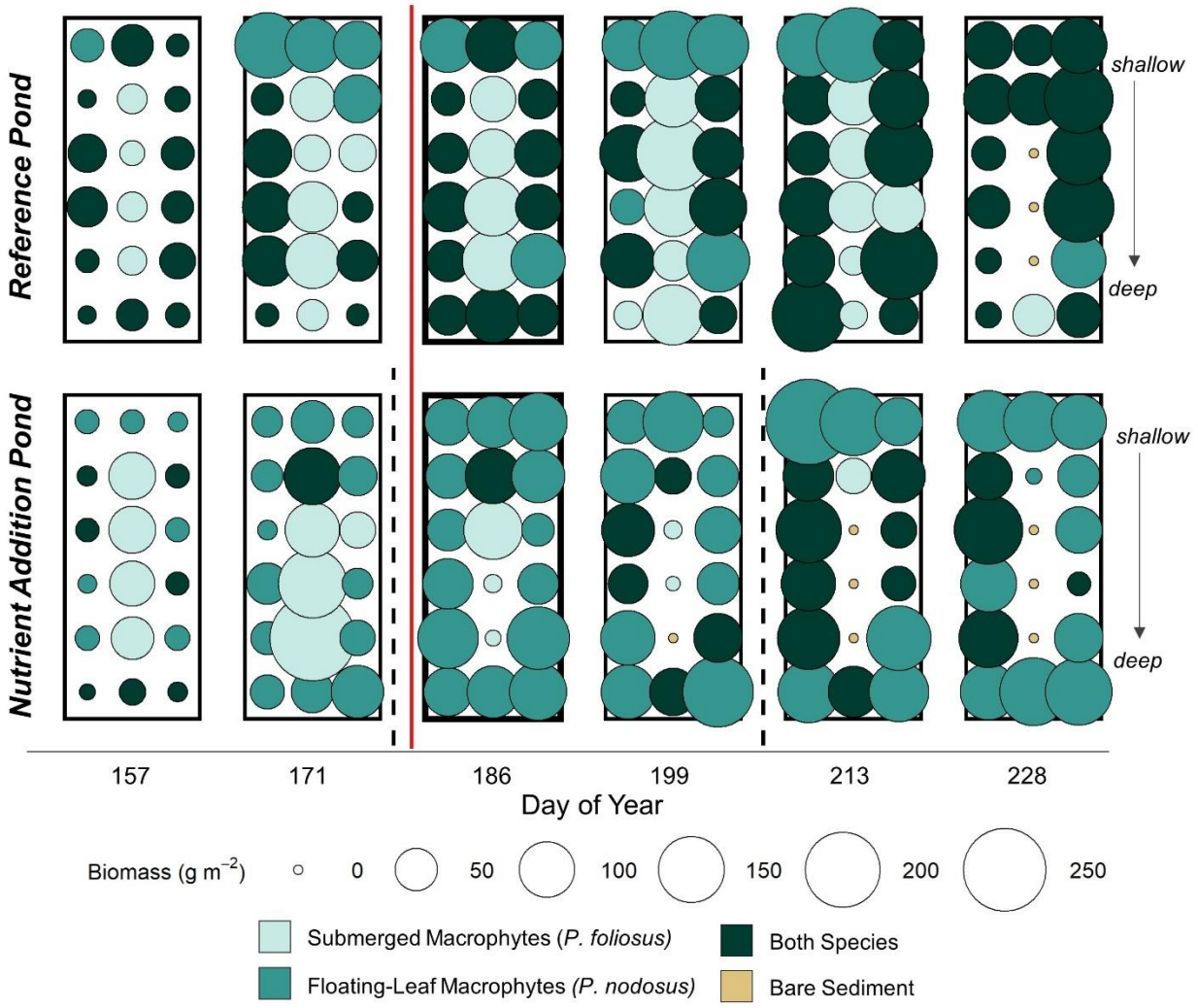

803

804 **Figure 3.** Spatial and temporal variation in macrophyte dry biomass density and species
805 assemblage in the reference (top) and nutrient addition (bottom) ponds. The start of the aquatic
806 heat event on DOY 185 is noted with the solid, red line. Dashed lines mark nutrient additions on
807 DOY 176 and 211.

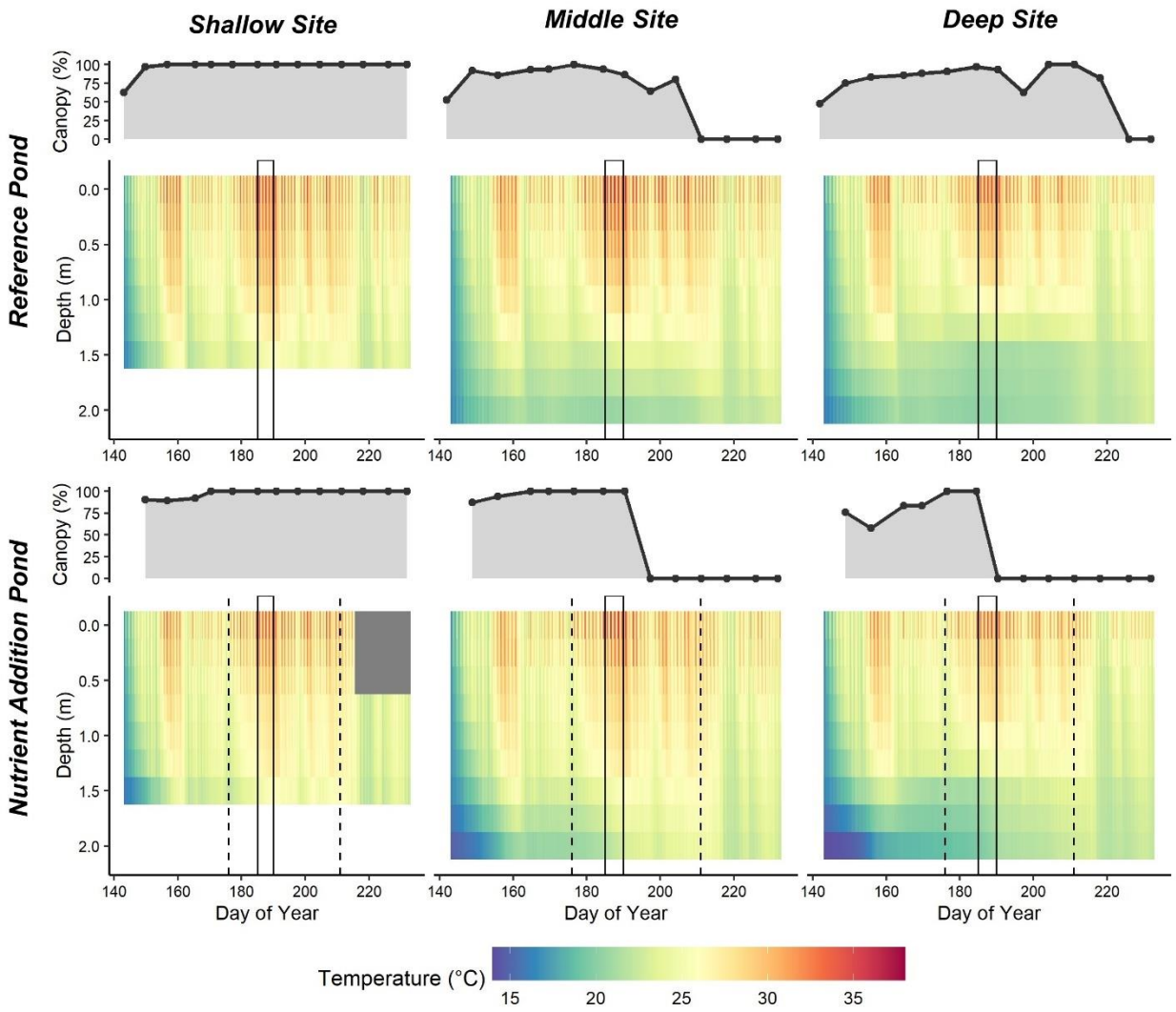

Figure 4. Spatial and temporal variation in macrophyte canopy height and temperature profiles. Canopy height is plotted as a percent of the water column height. Boxes mark an aquatic heat event from DOY 185-190 while dashed lines indicate nutrient additions on DOY 176 and 211. High frequency water temperature loggers were placed every 0.25 m of the water column up to 1.5 m and then every 0.5 m to the bottom. Temperature values at 1.75 m were interpolated for the sake of visualization. Several surface sensors (0-0.5 m) from the shallow site of the nutrient addition pond lost power following DOY 215 (grey box). An initial canopy height measurement is missing from the nutrient addition pond because the water was not sufficiently clear to see and measure the top of the canopy. The canopy height was less than 1 m or 50-75% of the water column at this time.

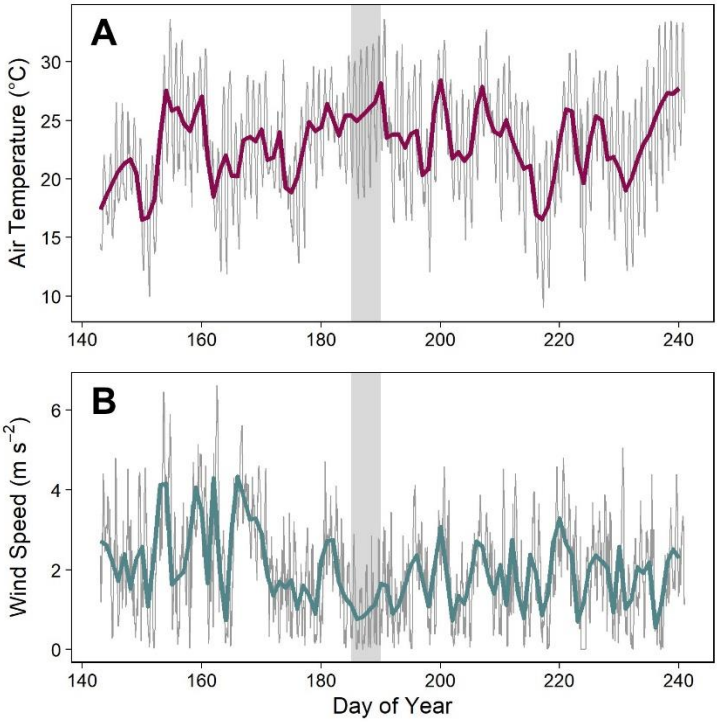

Figure 5. Air temperature (A) and windspeed (B) over the study period. Daily mean values are plotted in thicker lines over the hourly time series. The light grey box marks the aquatic heat event from DOY 185-190.

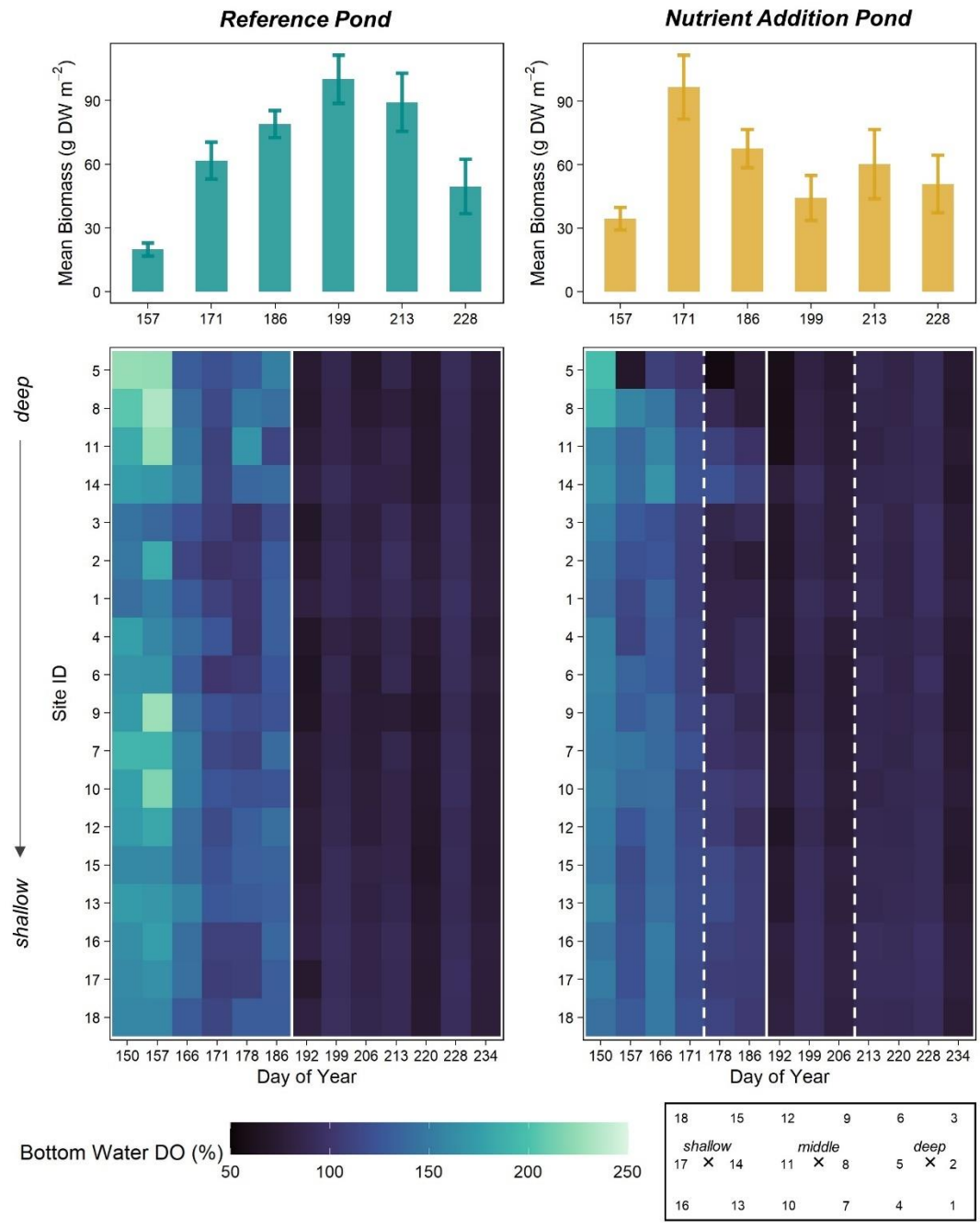

Figure 6. Pond averaged macrophyte dry biomass density over time (top panels) and spatiotemporal variation in bottom water dissolved oxygen (DO) saturation (bottom panels). Error bars on the macrophyte biomass bar plots represent the standard error of the mean. DO saturation values are reported by sampling site and date. Sampling sites are ordered approximately from the deepest to most shallow locations. A simplified map of sampling site location is displayed in the lower righthand corner of the figure. Data from sampling events before and after the end of the heat event (DOY 185-190) are separated with a solid white line. Dashed white lines indicate nutrient additions on DOY 176 and 211.

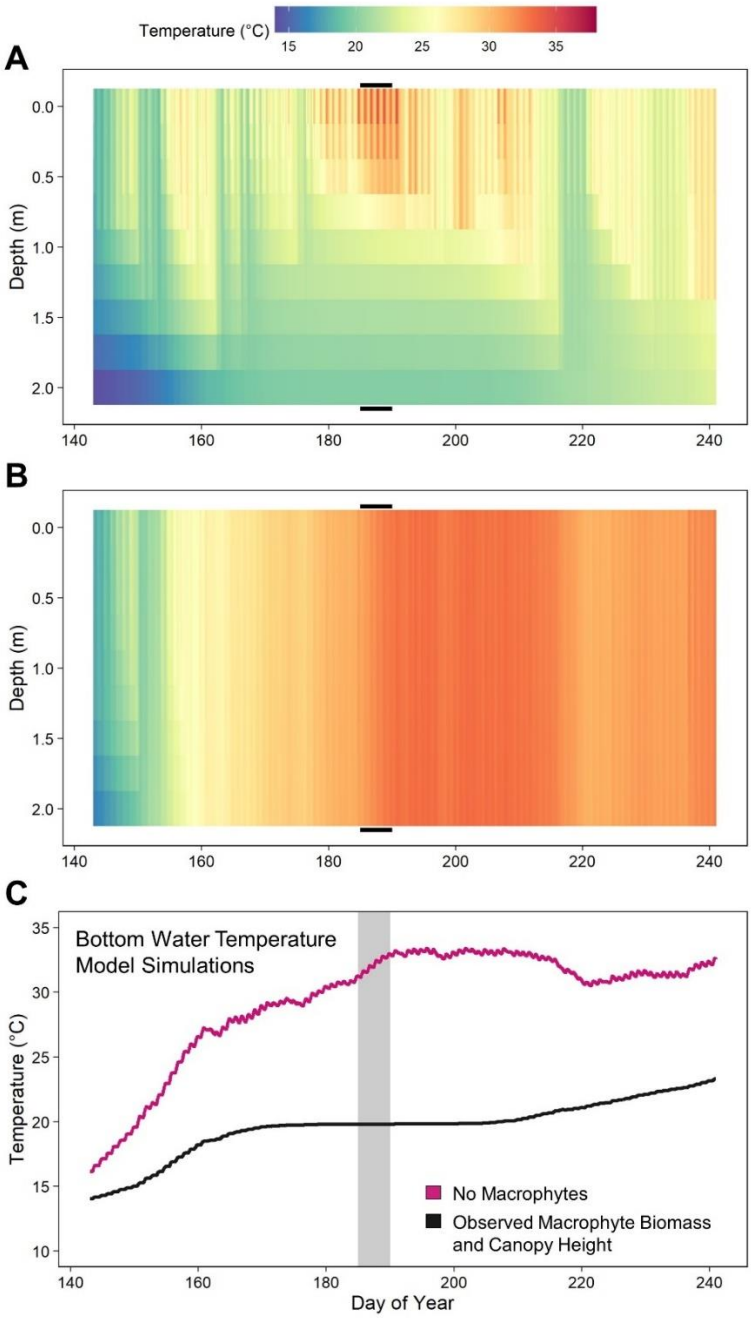

Figure 7. Model simulation results contrasting a no macrophyte scenario with the observed macrophyte coverage from the reference pond. Predicted temperature profiles with (A) observed macrophyte biomass and canopy height versus (B) no macrophytes present in the reference pond. Black, horizontal lines mark an aquatic heat event (DOY 185-190). (C) Timeseries of predicted daily mean bottom water (2m) temperatures with no macrophytes versus observed macrophyte biomass and canopy height.

Appendix S1

Influence of macrophytes on stratification and dissolved oxygen dynamics in ponds

Ellen A. Albright[1,2], Robert Ladwig[2], and Grace M. Wilkinson[1,2]

[1] Iowa State University, Ames, Iowa, USA

[2] Center for Limnology, University of Wisconsin-Madison, Madison, Wisconsin, USA

Corresponding author: Ellen A. Albright (ealbright2@wisc.edu)

Introduction

The appendix contains additional methods text detailing the algorithms and approach for the hydrodynamic model as well as an overview of calibrated model parameters (Table S1) and simulation input data for testing heat event response under variable macrophyte scenarios (Table S2). Model fit is illustrated in Figure S6.

Figure S1 provides an example of individual dissolved oxygen (DO) saturation profiles to illustrate there was no evidence of mid-depth DO maxima. Figure S2 shows a qualitative comparison in the change in macrophyte biomass during the summer at the central sampling sites across all the experimental ponds at the Iowa State University Horticulture Research Station. We provide time series of estimated thermocline depth (Figure S3) for each pond as well as time series of bottom water temperatures at each sampling site on each pond (Figure S4). We further provide supplementary visualizations for our DO data, specifically time series of surface and bottom water DO saturation and the difference between surface and bottom water DO (Figure S5).

Model Equations and Approach

Model description

A one-dimensional, integral energy model was developed to simulate the temperature, heat flux and stratification dynamics in small, vegetated ponds. Model algorithms are based on the MINLAKE model (Ford and Stefan ,1980; Riley & Stefan, 1988; Herb & Stefan, 2004).

Heat transport is implemented through the one-dimensional temperature diffusion equation:

(Eq. 1) $$\frac{\partial T}{\partial t} = \frac{\partial}{\partial z}\left(K_z \frac{\partial T}{\partial t}\right) + \frac{H(z)}{\rho_w c_p} + \frac{H_{geo}(z)}{\rho_w c_p}$$

where K_z is the vertical turbulent diffusion coefficient, H is internal heat generation due to incoming solar radiation, ρ_w is water density, c_p is specific heat content of water, and H_{geo} is internal geothermal heat generation.

Internal heat generation is implemented as:

(Eq. 2) $$H(z) = (1-\alpha) I_s^{-((k_d+k_m)z)}$$

where α is the water albedo, I_s is total incident short-wave radiation, and k_d is a light attenuation coefficient and k_m is the light attenuation coefficient due to macrophyte biomass.

For the upper, surface boundary condition we assume a Neumann type for the temperature diffusion equation:

(Eq. 3) $$H_{net} = \rho_w c_p \left(K_z \frac{\partial T}{\partial t}\right)$$

where H_{net} is the net heat flux exchange between atmosphere and water column:

(Eq. 4) $$H_{net} = H_{lw} + H_{lwr} + H_v + H_c$$

where H_{lw} is the incoming long-wave radiation, H_{lwr} is emitted radiation from the water column, H_v is the latent heat flux, and H_c is the sensible heat flux. Implementations to estimate the respective heat fluxes were taken from Livingstone and Imboden (1989) and Goudsmit et al. (2002). Latent and sensible heat fluxes were calculated using the atmospheric stability algorithms from Verburg and Antenucci (2010).

The lower, sediment boundary condition was prescribed as:

(Eq. 5) $$\left(K_z \frac{\partial T}{\partial t}\right) = 0$$

The model algorithm is modularized into three components: (a) heat generation from boundary conditions and vertical diffusion, (b) turbulent mixing up to the mixed layer depth, and (c) convective overturn to account for density instabilities.

(a) Heat generation from boundary conditions and vertical diffusion

In the first step the heat fluxes H and H_{geo} are applied over the vertical water column. The atmospheric heat flux, H_{net}, is applied to the surface layer.

Simultaneously, vertical turbulent diffusion between adjacent grid cells is calculated. Here, we applied the implicit Crank-Nicholson scheme. The vertical turbulent diffusion coefficient K_z is calculated based on the empirical equations by Hondzo and Stefan (1993) for lakes in Minnesota as a function of the buoyancy frequency:

(Eq. 6) $$K_z = a_k (N^2)^{-0.43}$$

where a_k is an empirical factor accounting for the surface area of the lake A_s:

(Eq. 7) $$a_k = 0.00706 (A_s)^{0.56}$$

and N^2 is the squared buoyancy frequency:

(Eq. 8) $$N^2 = \frac{g}{\rho_w} \frac{\partial \rho_w}{\partial z}$$

Values of N^2 less than 7.0 10^{-5} s^{-2} were set to 7.0 10^{-5} s^{-2}.

(b) Mixed layer depth

In the third step, we quantified the depth where the amount of external kinetic energy by wind shear stress equals the internal potential energy of the water column. Up to this mixed layer depth, z_{ml}, adjacent layers are subsequently mixed to account for a wind shear stress acting over the vertical water column. Here, the kinetic energy *KE* is described as:

(Eq. 9) $KE = \tau u^* \Delta t$

where τ is the surface turbulent shear stress, and u^* is the surface shear velocity, which was calculated from wind velocity as:

(Eq. 10) $u^* = \sqrt{\frac{C_{10}\rho_a}{\rho_w}} U_2$

where C_{10} is the wind stress coefficient dependent on the measured wind speed U_2 at 2 m height above the water surface, and ρ_a is the density of air, respectively (Herb and Stefan, 2005).

The dissipation of turbulent kinetic energy (DKE) by macrophytes is incorporated as:

(Eq. 11) $DKE_z = (\rho_w \hat{a} C_d)(u^*)^3 \Delta z \Delta t$

where $\hat{a}$ is the ratio of plant surface area per unit volume water and C_d is the plant form drag coefficient.

The potential energy of the water column for each layer over the depth is calculated as:

(Eq. 12) $PE_z = g Z_z (Z_{z+1} - Z_{cv}) \Delta \rho$

where g is gravitational acceleration, z_{cv} is the center of volume depth, and $\Delta\rho$ is a density change from the current layer to the next layer below.

The mixed layer depth z_{ml} is calculated by incrementally increasing the comparison between the difference of total kinetic energy *KE* to the dissipation of KE by macrophytes, and the internal potential energy *PE* as:

(Eq. 14) $z_{ml} \rightarrow PE_{z+1} > (KE - DKE_z)$

(c) Convective overturn

In the fourth step, any density instabilities over the vertical water column are mixed with a first stable layer below an unstable layer. Here, we applied an area weighed mean of temperature between adjacent layers to calculate the temperature of the mixed layer.

948 ***Appendix References***

949 1. Ford, D.E., and H.G. Stefan. 1980. Thermal predictions using an integral energy model. J.
950 Hydraul. Div. ASCE 106(1). 39-55, doi: 10.1061/JYCEAJ.0005358
951
952 2. Goudsmit, G.H., H. Burchard, F. Peeters, and A. Wüst. 2002. Application of k-e turbulence
953 models to enclosed basins: The role of internal seiches. J. Geophys. Res. 107. C12.
954 3230, doi:10.1029/2001JC000954
955
956 3. Herb, W.R., and H.G. Stefan. 2004. Temperature stratification and mixing dynamics in a shallow
957 lake with submersed macrophytes. Lake Reserv. Manag. 20(4): 296-308, doi:
958 10.1080/07438140409354159
959
960 4. Herb, W.R., and H.G. Stefan, 2005. Dynamics of vertical mixing in a shallow lake with
961 submersed macrophytes. Water Resour. Res. 41. W02023,
962 doi:10.1029/2003WR002613
963
964 5. Hondzo, M., and H.G. Stefan. 1993. Lake water temperature simulation model. J. Hydraul.
965 Eng. 119(11). 1251-1273, doi: 10.1061/(ASCE)0733-9429(1993)119:11(1251)
966
967 6. Livingstone, D., and D. Imboden. 1989. Annual heat balance and equilibrium temperature
968 of Lake Aegeri, Switzerland. Aquat. Sci. 51(4): 351-369, doi: 10.1007/BF00877177
969
970 7. Riley, M., and H.G. Stefan. 1988. MINLAKE: A dynamic lake water quality simulation
971 model. Ecol. Model. 43. 155-182, doi: 10.1016/0304-3800(88)90002-6
972
973 8. Verburg, P., and J.P. Antenucci. 2010. Persistent unstable atmospheric boundary layer
974 enhances sensible and latent heat loss in a tropical great lake: Lake Tanganyika. Journal
975 of Geophysical Research 115. 1-13. doi: 10.1029/2009JD012839

976

977

Table S1. *Calibrated model parameter values*

Variable	Description	Value	Parameterization
C_d	Wind momentum drag	0.0013	Calibration to field data
K_m	Macrophyte light extinction coefficient	0.04	Calibration to field data
$C_{d\ plant}$	Macrophyte momentum drag coefficient	1	Herb and Stefan (2004)
$\hat{a}$	Macrophyte area to volume	0.5	Calibration to field data
Wind factor	Wind speed multiplier	1	Best field calibration did not use wind speed or diffusion rate multipliers (so factors equal to 1)
Diffusion factor	Diffusion rate multiplier	1	
Short wave factor	Shortwave radiation multiplier	0.9	Calibration to field data
H_{geo}	Sediment heating coefficient	0	Calibration to field data
ρ_m	Macrophyte density	30	Calibration to field data

Table S2. *Input macrophyte data for model simulations*

Field Data – Reference Pond															
DOY	129	143	150	157	166	171	178	186	192	199	206	213	220	228	234
Canopy (m)	0.5	1	1.5	1.6	1.6	1.6	1.6	1.6	1.45	1	1.6	1.8	1/4	0.5	0.5
Biomass (g m^2)	NA	NA	NA	14.5	NA	48.4	NA	101.4	NA	73.6	NA	15.4	NA	22.4	NA
Simulation – No Macrophytes in Reference Pond															
DOY	129	143	150	157	166	171	178	186	192	199	206	213	220	228	234
Canopy (m)	0	0	0	0	0	0	0	0	0	0	0	0	0	0	0
Biomass (g m^2)	0	0	0	0	0	0	0	0	0	0	0	0	0	0	0

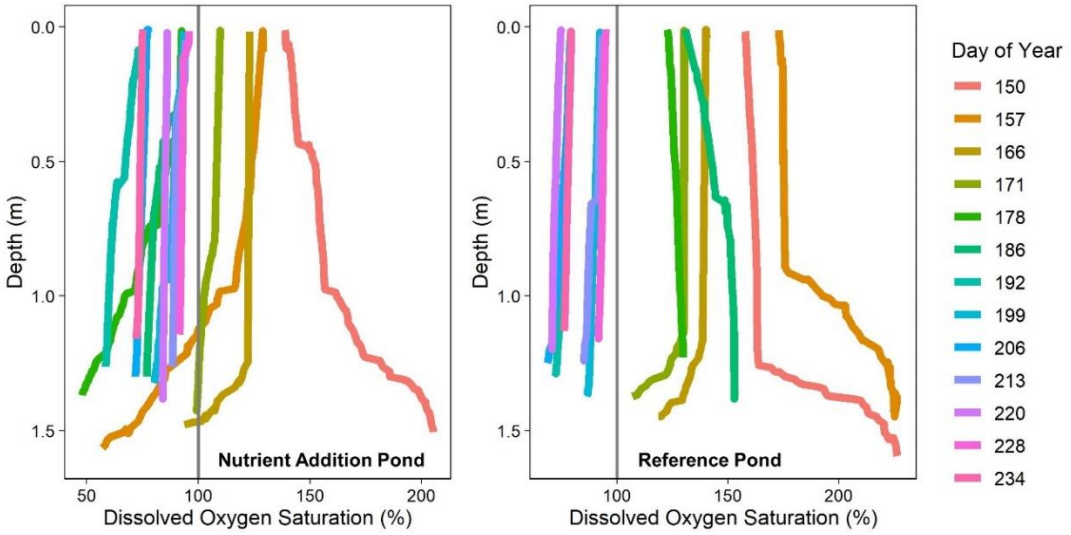

Figure S1. Examples of individual dissolved oxygen (DO) saturation profiles near the deep site of each study pond. Profiles are color-coded by the day of year (DOY) of the sampling event. These profiles were taken in the deeper, central region of the ponds. The vertical grey line highlights 100 percent saturation. The vertical distribution of DO saturation was either uniform, highest in the surface waters, or highest in the bottom waters depending on the time of year. There was no evidence of mid-depth DO maxima.

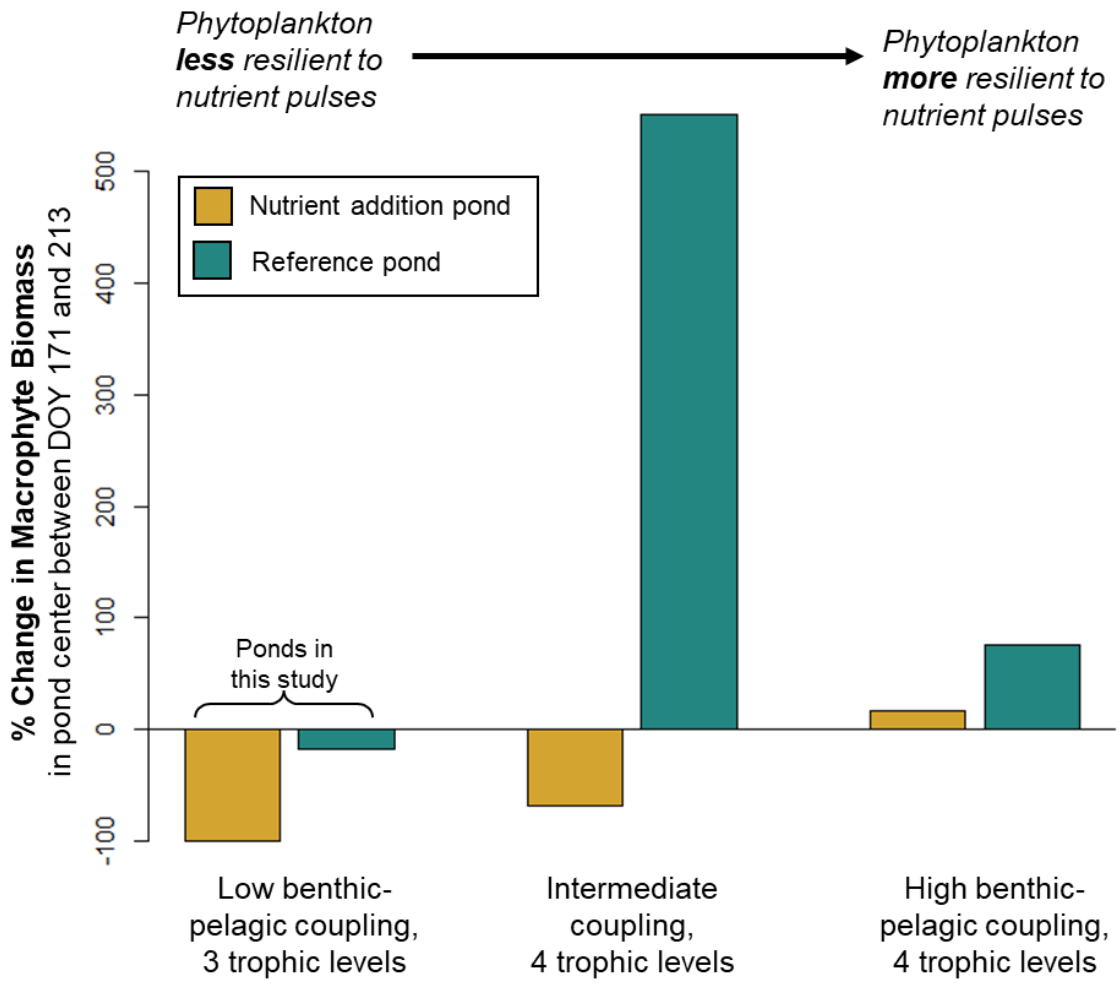

Figure S2. Change in macrophyte biomass during the summer at the central sampling sites in all the experimental ponds at the Iowa State University Horticulture Research Station. A total of six ponds are located at the station and were used in an experiment examining the role of food web structure (i.e., benthic-pelagic coupling) on phytoplankton resilience to nutrient pulses (Butts, 2023). One pond in each food web pair received a nutrient addition on DOY 176 and 211, as described in the main text. The two ponds with low benthic-pelagic coupling food webs were instrumented with high frequency sensors and used in this study. Less frequent macrophyte biomass measurements were taken in the other four ponds, all of which were more resilient to nutrient additions (i.e., less susceptible to light limitation stress). All ponds experienced the heat event from DOY 185-190. The pattern of early macrophyte senescence was most pronounced in this low coupling pond that received the nutrient additions, but also occurred in the intermediate coupling pond. In the high coupling pond, macrophyte biomass increased slightly in the nutrient addition pond (there was minimal increase in phytoplankton biomass in this treatment; Butts, 2023), but the increase was small, especially compared to the reference ecosystem during the same period. In summary, the ponds that received nutrient additions had a similar trajectory of declining or lower biomass earlier in the summer as compared to the reference ponds.

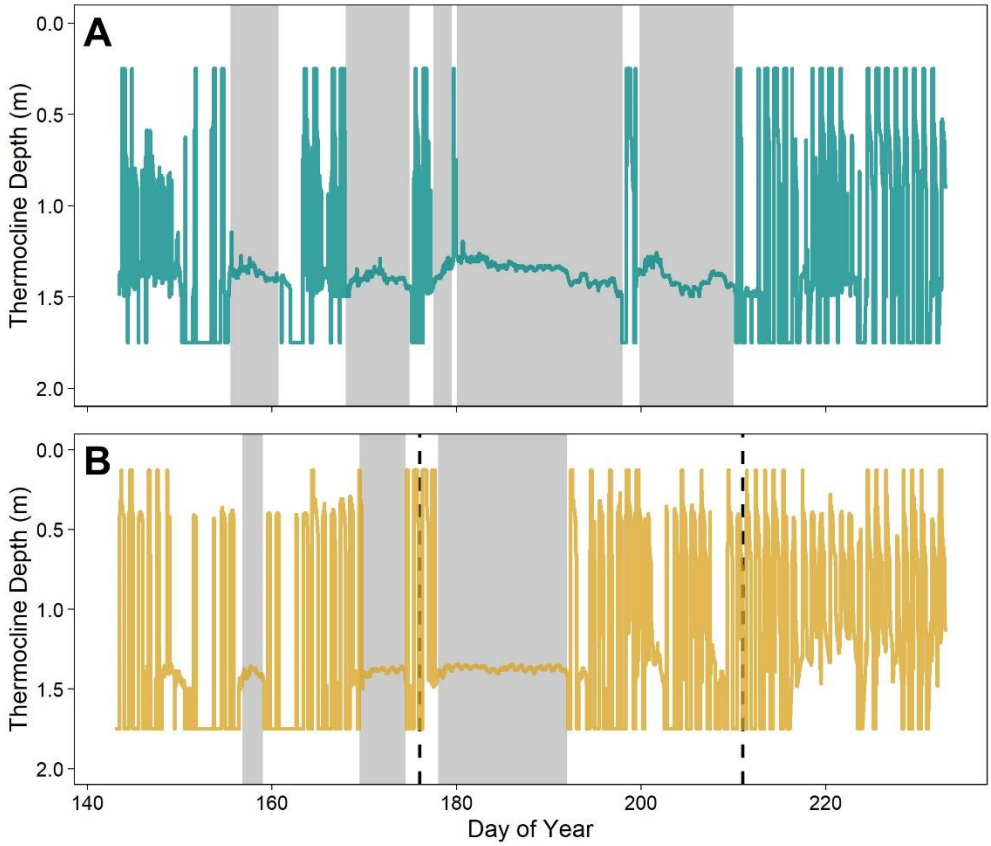

Figure S3. Estimated thermocline depth by pond. Periods of a stable thermocline for the reference (A) and nutrient addition (B) ponds are noted in the grey shaded boxes. Nutrient additions are noted with dashed black lines. Estimated thermocline values oscillating rapidly between the near surface and bottom waters were not considered time of stable stratification. A stable thermocline between 1-1.5 m depth was observed in the reference pond between DOY 155-161, and almost constantly between DOY 168-210, while the thermocline in the nutrient addition pond was more intermittent (DOY 157-159, 170-174, and 178-192).

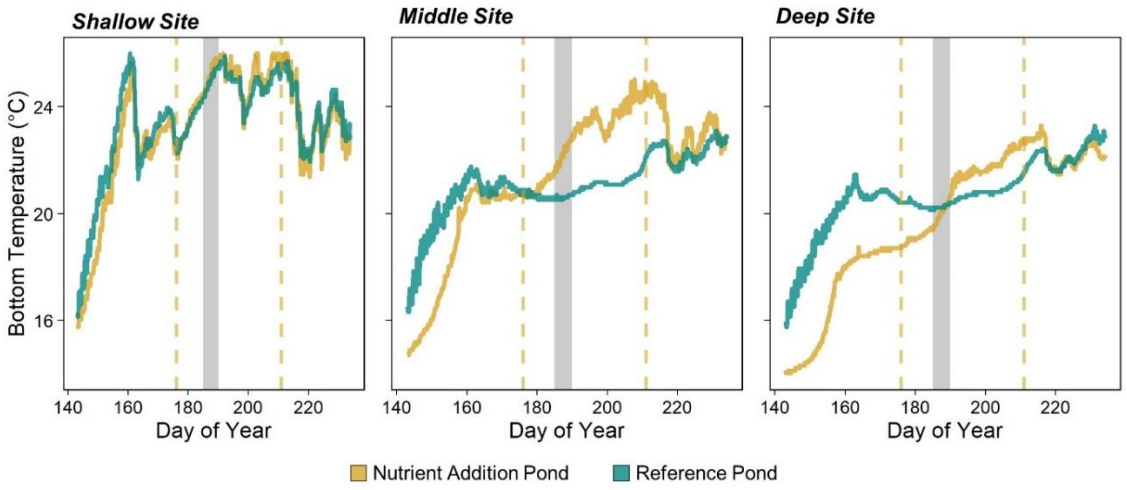

Figure S4. Bottom water temperature time series across sampling sites in each study pond. The grey box marks an aquatic heat event from DOY 185-190. Yellow dashed lines indicate the nutrient additions on DOY 176 and 211. During the heat event, bottom water temperature remained consistent at both the deep and middle sites of the reference pond. In contrast, bottom water temperatures in the nutrient addition pond increased by 1.3 °C and 1.4 °C at the deep and middle sites, respectively. At the shallow site in both ponds bottom water temperatures increased 1-1.3 °C during the heat event, suggesting an interaction with water depth.

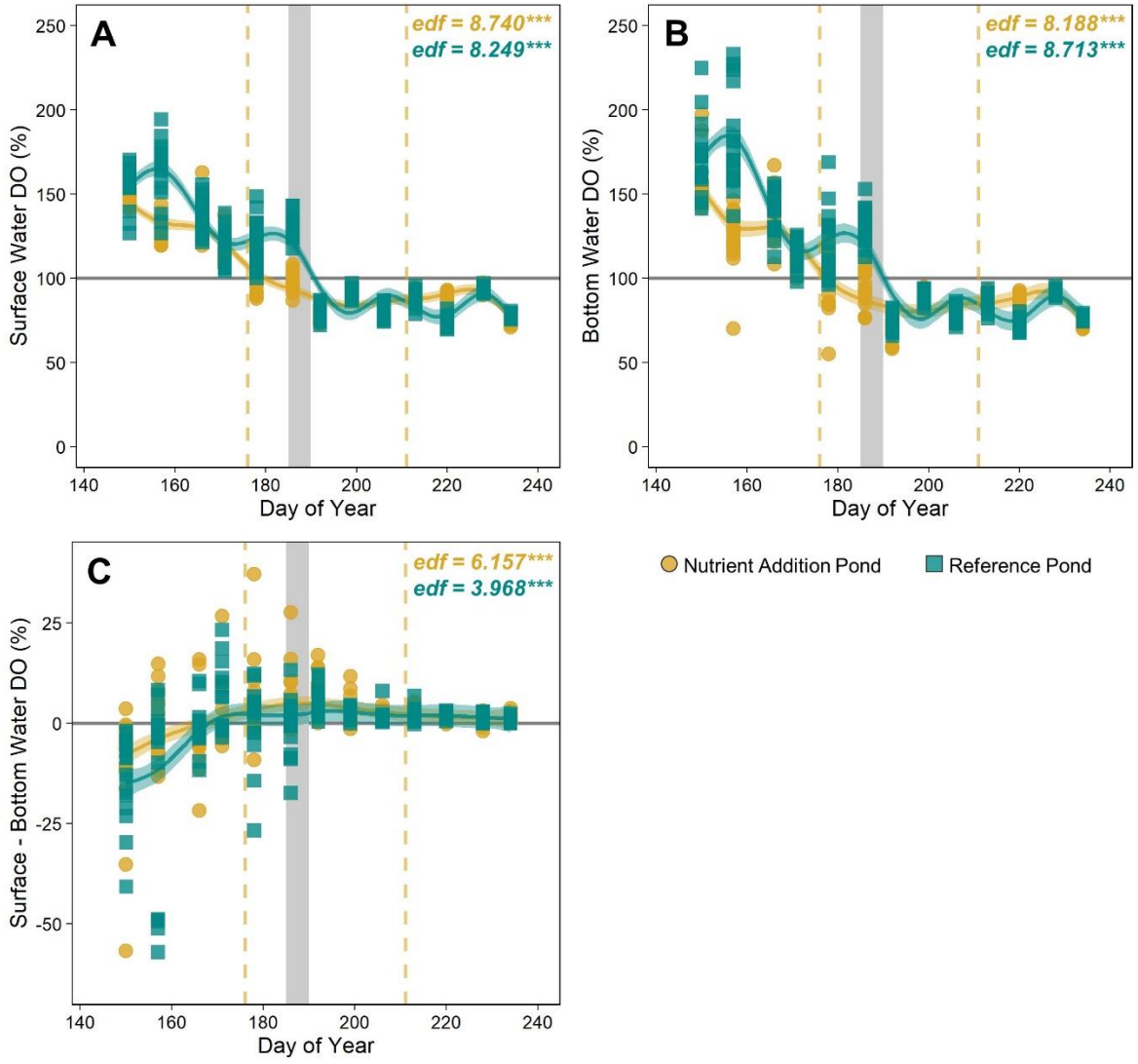

Figure S5. Time series of (A) surface and (B) bottom water dissolved oxygen (DO) saturation and (C) the difference between surface and bottom water DO saturation is based on weekly profiles at 18 sites across each pond. Negative values of delta-DO indicate greater DO saturation in the bottom waters while positive values mean DO is higher in the surface layer. Values from each pond were GAM-fit to highlight temporal trends. The asterisks next to the effective degrees of freedom (edf) correspond to the estimated p-value, with *** denoting $p < 0.001$. Across both panels, dashed yellow lines mark the timing of nutrient additions and the grey box highlights the aquatic heat event.

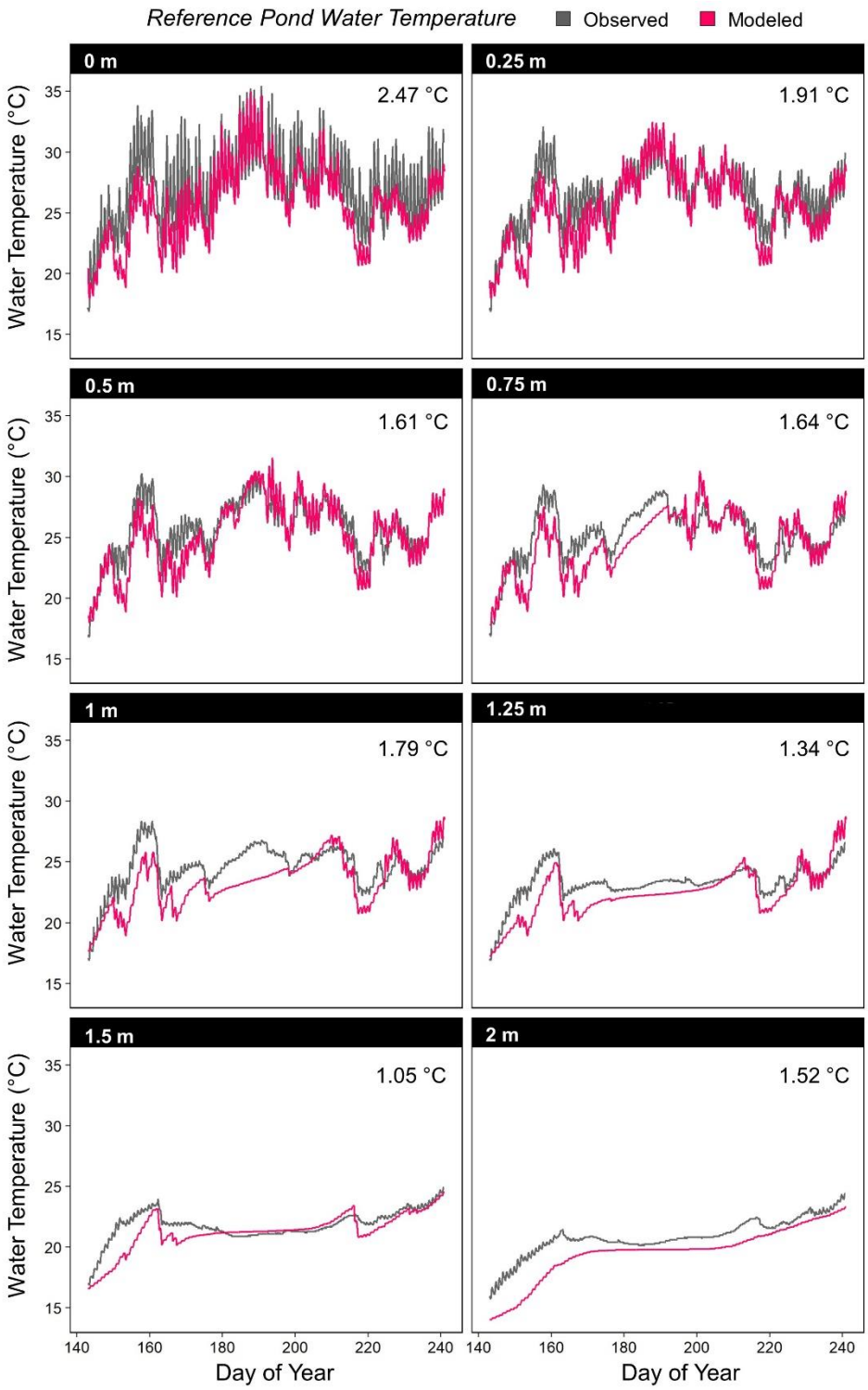

Figure S6. Model fit at discrete depths in the reference pond. Predicted water temperatures from the hydrodynamic model (pink lines) are plotted against the observed temperatures at the same depths (grey lines). The root mean square error (RMSE, °C) are noted in the top right corner of each panel. Overall, the model captured the magnitude and seasonal trends of temperature throughout the water column.